

Research Article

Parametric Design Method and Performance Analysis of Double S-Shaped Nozzles

Yong Shan ¹, Xiaoming Zhou,² Xiaoming Tan,¹ Jingzhou Zhang ¹ and Yanhua Wu³

¹Jiangsu Province Key Laboratory of Aerospace Power System, College of Energy and Power Engineering, Nanjing University of Aeronautics and Astronautics, Nanjing 210016, China

²AECC Commercial Aircraft Engine Co. Ltd, 200241, China

³School of Mechanical and Aerospace Engineering, Nanyang Technological University, Singapore

Correspondence should be addressed to Yong Shan; nuaasy@nuaa.edu.cn

Received 25 December 2018; Revised 20 February 2019; Accepted 10 March 2019; Published 12 May 2019

Academic Editor: Andre Cavalieri

Copyright © 2019 Yong Shan et al. This is an open access article distributed under the Creative Commons Attribution License, which permits unrestricted use, distribution, and reproduction in any medium, provided the original work is properly cited.

A parametric design method, which was based on super-elliptical transition and self-adaption infrared radiation shield for the double S-shaped nozzle, was introduced. The complete shielding of high-temperature components in the S-shaped nozzle was realized. Model experiments and numerical simulations were performed to investigate the effects of offset ratio S/D , the ratio of length to diameter L/D , and the aspect ratio W/H on the aerodynamics and infrared radiation. The results showed that the total pressure recovery and thrust coefficients were improved initially, but dropped rapidly with the increase in offset ratios with the range of investigated parameters. There existed an optimal offset ratio for the aerodynamic performances. Considering the weight penalty, the length of nozzles should only be increased properly to achieve better aerodynamic performances. Both friction and viscous losses caused by large streamwise vortices dominated the aerodynamic performances of nozzles. The nozzle with the aspect ratio of $W/H = 5.0$ was recommended for achieving optimal aerodynamics. The increase in aspect and offset ratios could effectively suppress plume radiation, which was, however, not sensitive to overall radiation. Compared to circular nozzles, double S-shaped nozzles reduced overall infrared radiation by over 50%, which proves significant stealth ability. A balance between aerodynamic performances and infrared radiation suppression could be reached for double S-shaped nozzles.

1. Introduction

Booming development of technologies in infrared detection for infrared signatures has severely threatened aircraft powered by aero-engines, one of which is the portable infrared radiation (IR) seeking missiles for military use [1]. In order to improve the survivability of aircraft, many countermeasures were taken for suppressing IR signatures [2]. It is considered that the exhaust system of engine is the most important radiation source in the near infrared band, and most aircraft with a function of stealth must deploy a low-level IR signature nozzle [3].

For an axisymmetric convergent-divergent nozzle, high-temperature units, such as center plug, flame holder, liner, and strut, are exposed of a considerable radiation intensity at some particular lines of sight. Various cooling technologies have been effectively applied to lower down temperatures of

these hot parts in the exhaust cavity. For instance, the two-dimensional convergent-divergent nozzle (2DCD) [4, 5] designed with infrared stealth function usually used film cooling to cool the flap and side walls. As well known, shielding of radiation is another effective way to decreasing IR signature which spreads from the cavity of the exhaust system. For example, the two-dimensional nozzle can shield part of radiation of the center plug and flame holder. The axis-symmetric plug nozzle can shield the entire radiation originating from the exhaust cavity. However, the plug immersed in the hot plume becomes a significant radiation source unless it can be cooled to a certain level. Infrared suppression consideration leads to serpentine nozzles to provide line-of-sight blockage of the exhaust system. For example, the highly efficient embedded turbine engine (HEETE) plan presented the serpentine inlet and exhaust nozzle, which could shield the fan and high-temperature

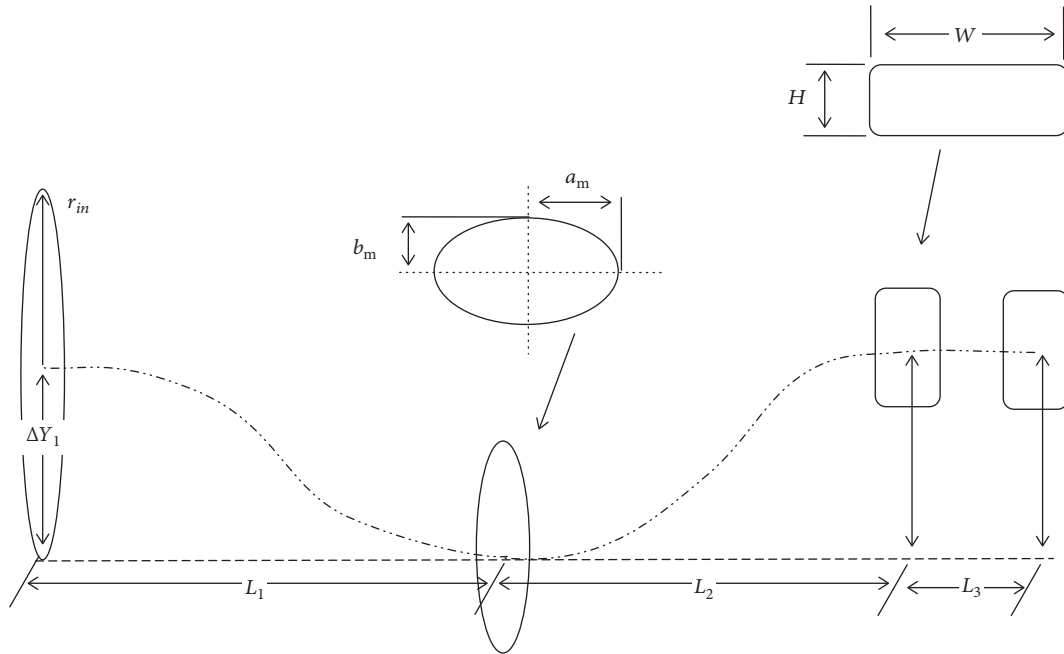


FIGURE 1: Design parameters of the double S-shaped nozzle.

cavity of the exhaust system from both radar and infrared radiation [6]. Many researchers paid more attention on the S-shaped nozzle to reduce IR signature levels. An et al. [7] analyzed the effects of S-shaped nozzle configurations of an unmanned aerial vehicle (UAV) and atmospheric conditions on plume IR signatures. It was found that infrared signature levels were reduced significantly in the axial direction. However, relatively higher signature levels were observed on the left and right sides and below the nozzle due to increase the aspect ratio of the nozzle outlet, as well as curvature, which led to a wider distribution of the plumes along a downward slope. Rajkumar et al. [8] performed an experiment to investigate the flow through a shallow single serpentine curved convergent nozzle with different pressure ratios. It revealed initial deceleration of the flow due to the turning of the streamlines caused by the nozzle curvature and the acceleration of the core flow due to geometric transition. Du et al. [9] numerically conducted the predictions of a lobed jet mixing flow within an S-shaped nozzle. Due to the use of the S-shaped nozzle, a sharp decrease in total pressure recovery coefficient, as well as a reduced thermal mixing efficiency, was shown. Gao et al. [10] used reverse the Monte-Carlo method to calculate the infrared radiation intensity of an axisymmetric nozzle and three S-shaped nozzles. The results showed that the infrared intensity of the S-shaped nozzle is much lower than that of the axisymmetric nozzle. The S-shaped nozzle can effectively reduce the maximum IR intensity in the rear hemispheric space. Liu et al. [11, 12] demonstrated the characteristics of the infrared radiation for a single-serpentine and a double-serpentine 2D nozzle. It was demonstrated that the serpentine nozzle could mask the high-temperature elements of the turbine section effectively, and the IR of the exhaust system was suppressed by 70% compared to the axisymmetric nozzle. Sun et al.

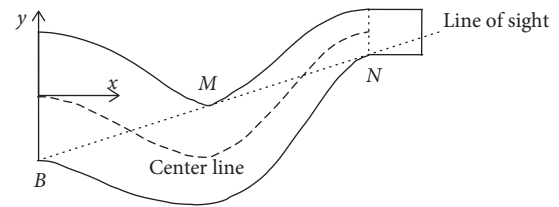


FIGURE 2: The geometric condition of complete shielding.

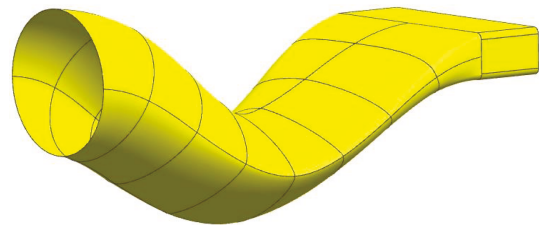


FIGURE 3: Schematic diagram of a double S-shaped nozzle.

[13] studied the influences of the design parameters on the aerodynamic performance of a double serpentine nozzle experimentally and numerically. Static pressure distributions on the upper and lower wall surfaces showed good agreement between the experimental data and computation. It showed that two-equation standard $k-\epsilon$ turbulence is accurate to reveal the aerodynamic performances. A further study of Sun et al. [14] presented a range of values of some important parameters for achieving better aerodynamic performances. Cheng et al. [15] investigated the influences of the shield ratio on the infrared signature for the serpentine nozzle. Numerical results show that 28.9% of the infrared radiation intensity can be reduced by the single serpentine nozzle compared

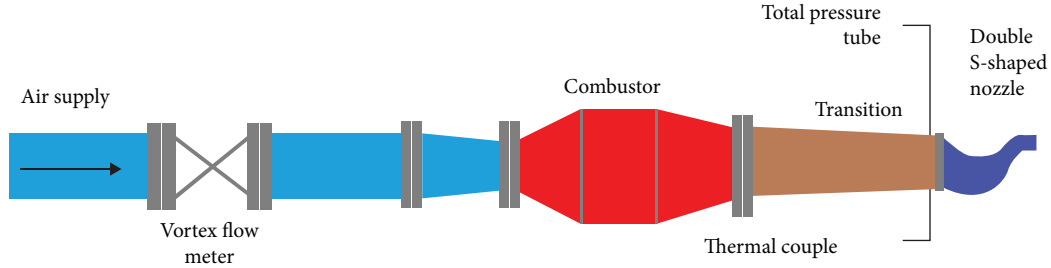


FIGURE 4: Schematic diagram of the experimental system.

with the circular nozzle. The shield ratio has little effect on the infrared signature of gas outside of the serpentine nozzle's exit.

From the literature above, the S-shaped nozzle is promising to suppress infrared radiation of the exhaust system [16–18]. However, it is inevitable to bring aerodynamic loss for serpentine flow passage. No matter what kinds of serpentine nozzles to choose, complete shielding in shape must be helpful to gain maximum stealth ability. Deep understanding of serpentine nozzles is beneficial to balancing various performances before the nozzle design. The aim of this study is to introduce a parametric method to conveniently obtaining the geometry of a double S-shaped convergent nozzle with complete shielding function. According to the method, a double S-shaped convergent nozzle can be designed quickly under the control of some key input parameters, such as aspect ratio W/H , offset ratio S/D , and the ratio of length to diameter L/D . Several selected experiments and numerical simulations were performed to investigate the effects of nozzle configurations on aerodynamic and infrared radiation characteristics of double S-shaped convergent nozzles.

2. Geometric Design Methods for the Double Serpentine Nozzle

2.1. Centerline and Area Distributions of Nozzles. Lee et al. [19] introduced three centerline distributions (rapid turning at the exit, rapid turning at the entrance, and modest turning) and three area distributions (rapid area change at the exit, rapid area change at the entrance, and modest area change) from inlet to outlet, which would produce better aerodynamic performances for the subsonic diffuser. Centerline shapes control the transverse pressure gradient which is responsible for secondary flow and flow loss. Area distributions control the streamwise pressure gradient which induced the flow separation. In this paper, a modest turning centerline equation shown in Equation (1) is used to obtain centerline coordination for the S-shaped nozzle. Similarly, a modest area change equation represented by Equation (2) is employed to acquire the section area of nozzles.

$$y = \Delta Y \left(3 \left(\frac{x}{L} \right)^2 - 2 \left(\frac{x}{L} \right)^3 \right), \quad (1)$$

where y denotes the vertical coordinate of the centerline, x represents the horizontal coordinate of the centerline, ΔY is the offset of nozzles, and L is the axial length.

$$\frac{A}{A_e} = \left(\frac{A_{in}}{A_e} - 1 \right) \left(3 \left(\frac{x}{L} \right)^2 - 2 \left(\frac{x}{L} \right)^3 \right) + 1, \quad (2)$$

where A_e and A_{in} are areas of S-shaped nozzle exit and entrance, respectively.

2.2. Geometrical Parameters of Transverse Sections. The geometrical parameters of the double S-shaped nozzle which transits from circle to rectangle are shown in Figure 1. The radius of nozzle inlet R_{in} fits the size of the turbine casing. Aspect ratio W/H is the ratio of width to height for the rectangle outlet. The total length L of the nozzle includes the first S-shaped segment with length L_1 , the second S-shaped segment with length L_2 , and the straight segment with length L_3 . At any transverse sections, the shape is super-elliptical with long axis a and short axis b . The total offset of nozzles can be described by $S = |\Delta Y_2 - \Delta Y_1|$. ΔY_1 is the offset of the first S-shaped segment. ΔY_2 is the offset of the second S-shaped segment, shown as Figure 1.

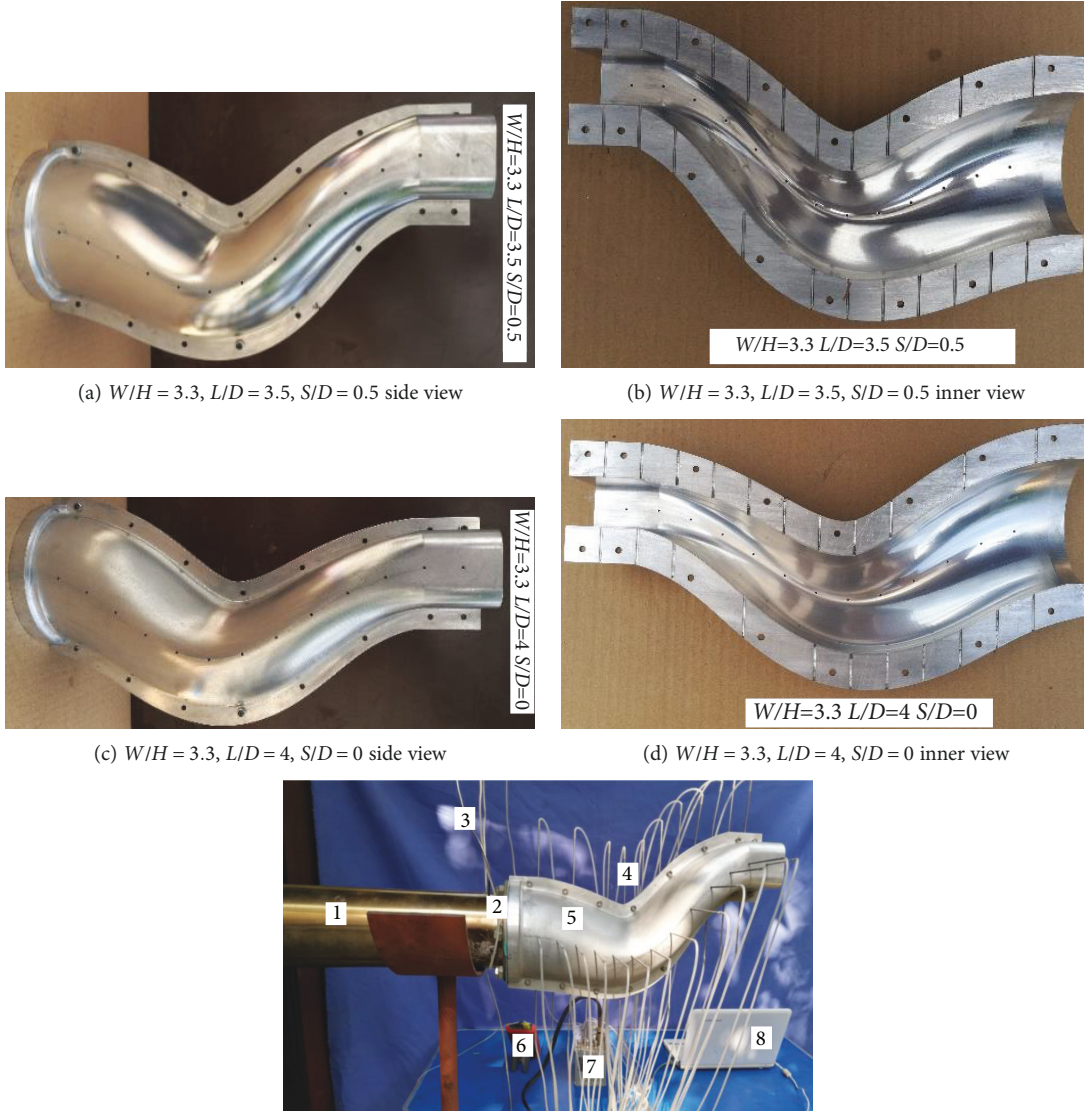
Firstly, according to pressure ratio and inlet area A_{in} of nozzles, the area A_e and equivalent radius R_e of the outlet rectangle can be obtained by isentropic expansion theory. On the assumption that any transverse section is elliptical, the long axis $a(x)$ and short axis $b(x)$ can be calculated by Equation (3).

$$\begin{bmatrix} a^2(x) \\ b^2(x) \end{bmatrix} = \left[3 \left(\frac{x}{L} \right)^2 - 2 \left(\frac{x}{L} \right)^3 \right] \begin{bmatrix} R_{in}^2 - a_e^2 \\ R_{in}^2 - b_e^2 \end{bmatrix} + \begin{bmatrix} a_e^2 \\ b_e^2 \end{bmatrix}, \quad (3)$$

where a_e and b_e are half lengths of the width and height of the rectangle outlet, respectively.

The area of super ellipse can be written by as

$$A = 4 \int_0^b x dy = 4 \int_0^b a \left[1 - \left(\frac{y}{b} \right)^n \right]^{1/n} dy, \quad (4)$$



(e) Nozzle with pressure probes. (1) Transition section, (2) total pressure tube, (3) thermal couple, (4) static pressure tube, (5) double S-shaped nozzle, (6) temperature scanner, (7) pressure scanner, and (8) laptop

FIGURE 5: Photo of double S-shaped nozzles.

where n is the exponent of the super ellipse. Combining Equation (3) and Equation (4), the exponent of super ellipse n can be well-determined by iteration with the dichotomy method.

2.3. Geometric Constraint of Line-of-Sight Blockage. The coordinate system in this paper is shown as Figure 2. The coordinate of points B , M , and N can be described as $(0, -R)$, $(L_1, b_m - \Delta Y_1)$, and $(L_1 + L_2, \Delta Y_2 - \Delta Y_1 - 1/2H)$, respectively. To provide line-of-sight blockage of the exhaust system, the points of B , M , and N should be collinear which can be represented in Equation (5).

$$\frac{b_m - \Delta Y_1 + R}{L_1} = \frac{\Delta Y_2 - \Delta Y_1 - (1/2)H_e - b_m + \Delta Y_1}{L_2 + L_1 - L_1}. \quad (5)$$

TABLE 1: Geometric parameters of experimental nozzles.

W/H	S/D	L/D
3.3	0	3.0
3.3	0	3.5
3.3	0	4.0
3.3	0.5	3.5
3.3	1.0	3.5

Next, Equation (5) can be rewritten to become

$$\Delta Y_2 + \frac{L_2}{L_1} \Delta Y_1 = \left(\frac{L_2}{L_1} + 1 \right) b_m + \frac{L_2}{L_1} R + \frac{1}{2} H_e. \quad (6)$$

TABLE 2: Geometric parameters of computational nozzles.

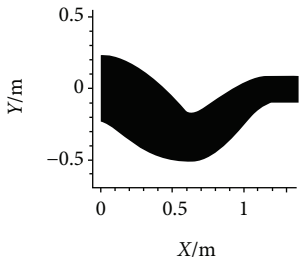
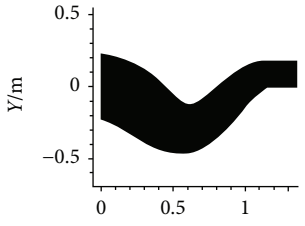
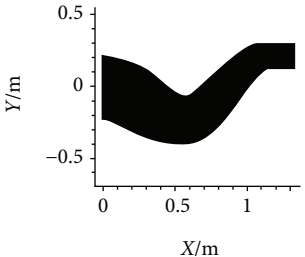
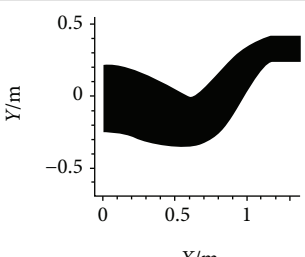
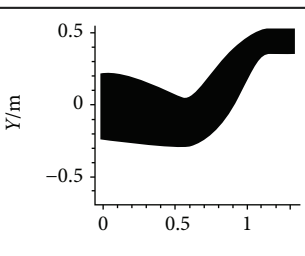
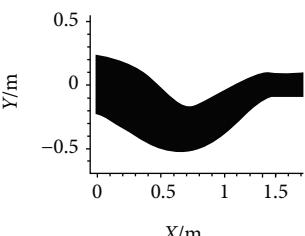
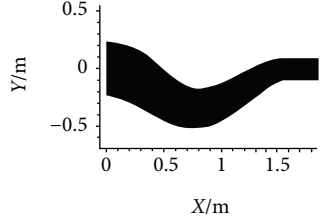
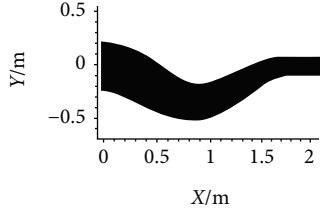
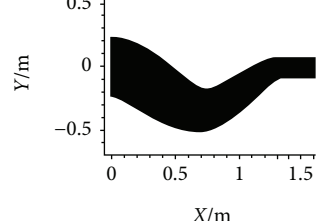
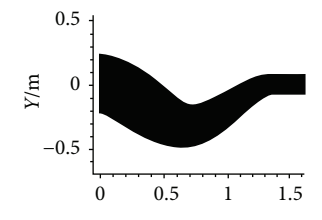
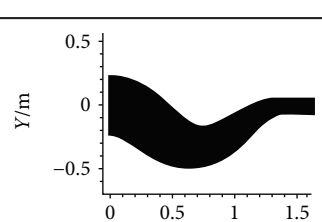
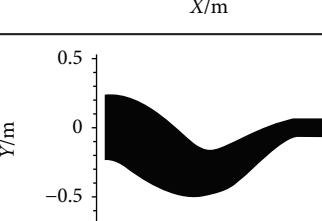
Model	L/D	S/D	W/H	Outline
1 (baseline)	3.0	0	3.3	
2	3.0	0.25	3.3	
3	3.0	0.5	3.3	
4	3.0	0.75	3.3	
5	3.0	1.0	3.3	
6	3.5	0	3.3	

TABLE 2: Continued.

Model	L/D	S/D	W/H	Outline
7	4.0	0	3.3	
8	4.5	0	3.3	
9	3.5	0	4.15	
10	3.5	0	5.0	
11	3.5	0	5.85	
12	3.5	0	6.7	

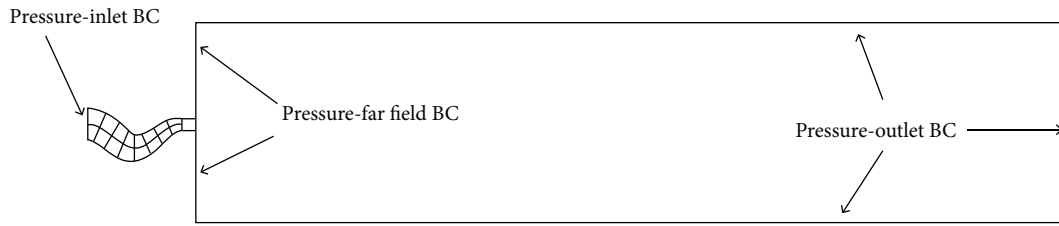


FIGURE 6: Boundary conditions.

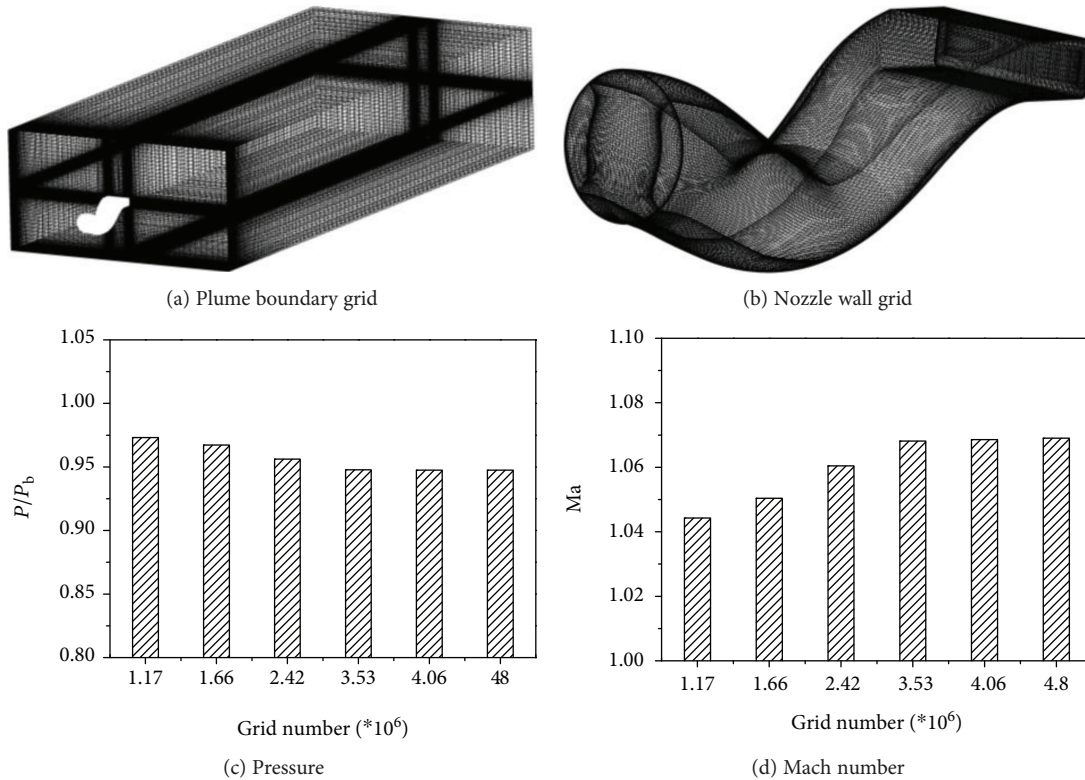


FIGURE 7: Schematic computational grids and grid independency.

Combining with Equation (7) below, ΔY_1 and ΔY_2 can therefore be obtained.

$$S = |\Delta Y_2 - \Delta Y_1|. \quad (7)$$

Following the parametric design method, a double S-shaped nozzle which is shown in Figure 3 can be structured with the inlet circle, outlet rectangle, and a few of super ellipses between inlet and outlet.

3. Experimental Procedures

An experimental system was established, including gas supply, flow meter, combustor, various double S-shaped nozzles, and data acquiring instruments, to acquire the nozzle wall pressure distributions (shown in Figure 4) and infrared radiation of nozzles. The airflow which was supplied by an electrical single-stage compressor was heated in a combustor with aviation fuel. The flow rate is 12 kg/min, and the temperature is 440 K. The infrared FT spectroradiometer

produced by BOMEM Company in Canada, which responds in the spectral range of $3 \mu\text{m}$ - $5 \mu\text{m}$ and $8 \mu\text{m}$ - $14 \mu\text{m}$, was used to measure the $3 \mu\text{m}$ - $5 \mu\text{m}$ radiance intensity of nozzles. To acquire static pressure of the side and upper wall of nozzles, twenty-six electronic pressure transducers were used in the aerodynamic experiment. These pressure measurements were made at locations of $x/L = 0.071, 0.143, 0.214, 0.286, 0.357, 0.429, 0.500, 0.571, 0.643, 0.714, 0.785, 0.857,$ and 0.929 , along the centerline of the nozzle, which can be seen in Figure 5(e). L is the total length of experimental nozzles, $x/L = 0$ is at the inlet of nozzles, and $x/L = 1$ is at the outlet of nozzles. The pressure transducers are of type 9116 produced by TE Connectivity Ltd. And they have an accuracy of $\pm 0.05\%$ FS (full scale). To improve the accuracy of the pressure measurements, the weighted average value of static pressures was adopted. The uncertainty estimate of pressure is about ± 0.25 Psi.

To accommodate various offset ratios (S/D), ratios of length to diameters (L/D), and same outlet aspect ratios (W/H), as shown in Table 1, five double S-shaped nozzles

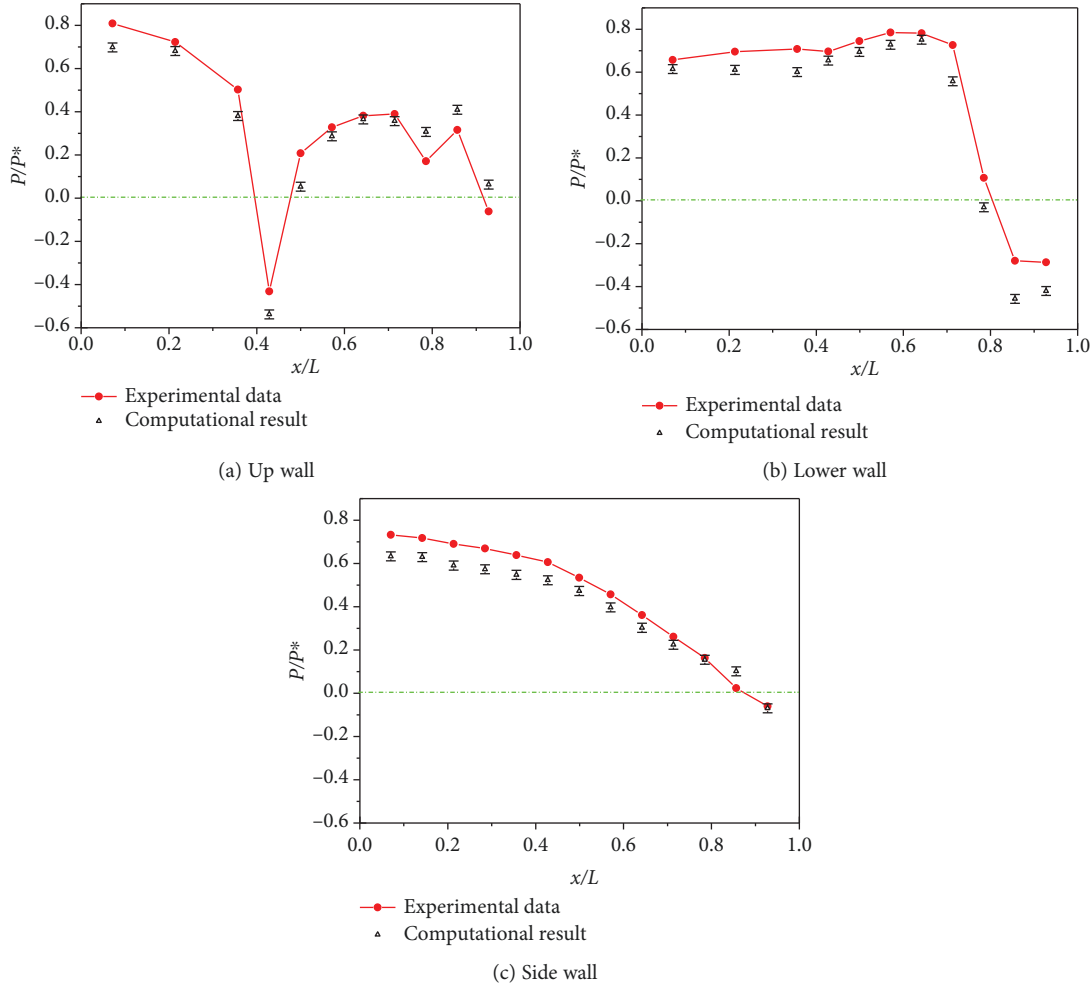


FIGURE 8: Comparison of experimental and computational results ($S/D = 1$, $L/D = 3.5$).

were designed and manufactured for aerodynamics experiments. Photos of two nozzles for the experiments are shown in Figure 5.

4. Numerical Procedures

4.1. Numerical Models and Boundary Conditions. A series of nozzles were designed with the method mentioned above to understand the effects of important geometric parameters on aerodynamic performances. Table 2 shows twelve double S-shaped nozzles with different W/H , S/D , and L/D ratios.

The exhaust flow region which can be seen in Figure 6 is necessary to obtain the sufficient information on exhaust flow and accurate aerodynamic analysis. After some attempts, the height and width of the exhaust flow region are about ten and three times that of the nozzle outlet, respectively. The length of the exhaust flow region is about thirteen times that of nozzles.

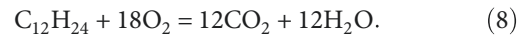
The boundary conditions of computational domain were specified as follows:

- (1) Inlet boundary: the inlet of the nozzle was defined as the pressure inlet with $P^* = NPR \times 22700$ Pa, $T^* = 440$ K. Here, the NPR, which denotes the ratio

of the nozzle inlet pressure to atmosphere pressure, is 1.5. To simulate the local conditions of nozzles under flight, a stream of flow parallel to the nozzles was set as pressure far field with Mach number as 0.7

- (2) Outlet boundary: the flow outlet which was located at the exhaust flow region was set as the pressure outlet with atmosphere pressure of $P_b = 22700$ Pa, and temperature of $T_b = 216$ K, corresponding to the environment of an altitude of 11 km
- (3) Wall boundary: the no-slip condition was applied to all solid walls in the numerical region

On the assumption that the inlet flow of nozzles is full burnable, it consists of nitrogen, carbon dioxide, and vapor. The chemistry reaction formula is as follows:



The volume percentage of nitrogen, carbon dioxide, and vapor is set as 69.3%, 6.14%, and 24.56%, respectively, at the flow inlet. The surrounding atmosphere is with nitrogen of 79% and oxygen of 21%.

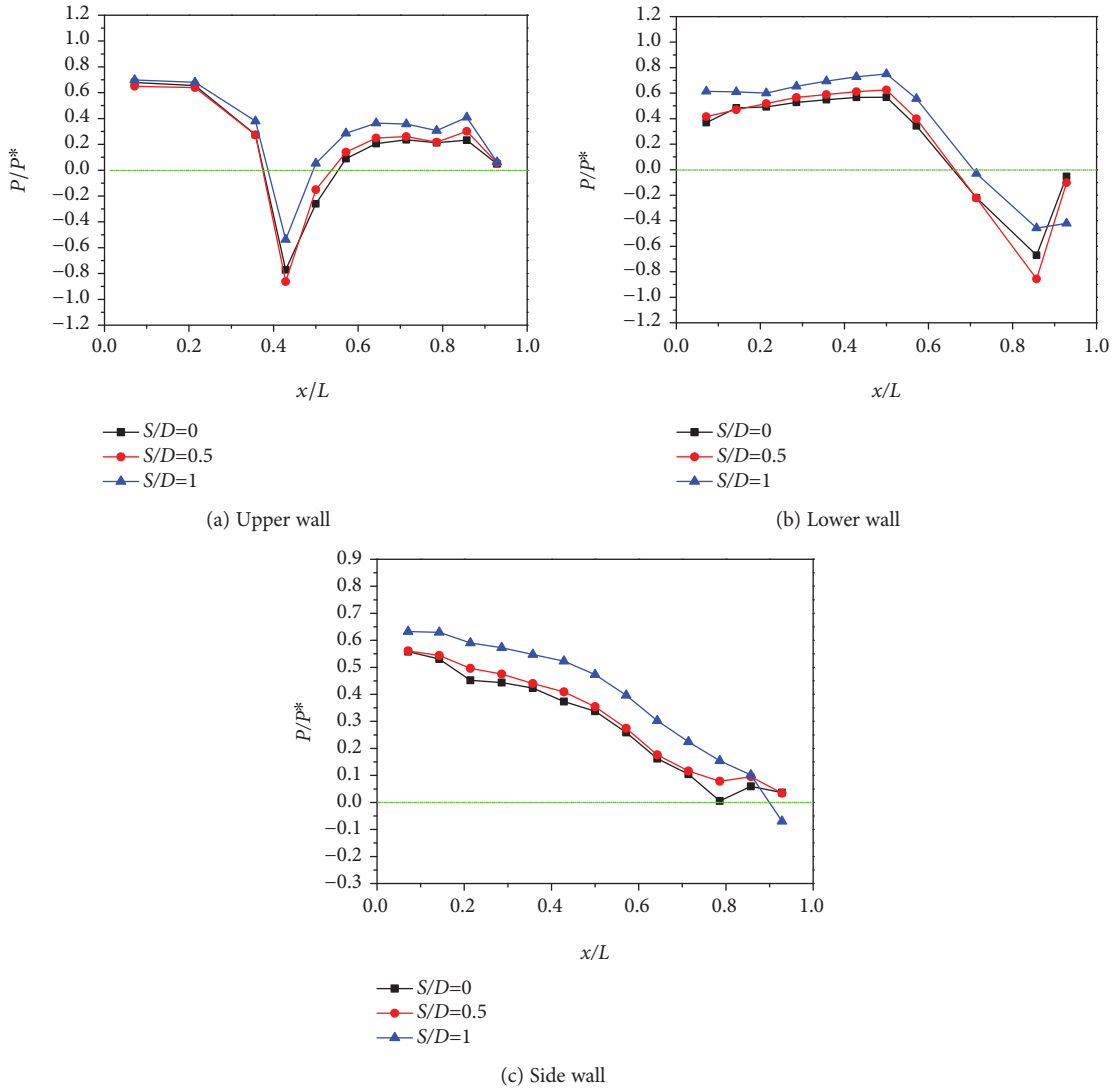


FIGURE 9: Effects of offset ratios on wall pressure.

4.2. *Numerical Method and Meshes.* The standard $k-\epsilon$ turbulent model, renormalization group (RNG) $k-\epsilon$ turbulent model, realizable $k-\epsilon$ turbulent model, standard $k-\omega$ turbulent model, and SST $k-\omega$ turbulent model were compared in the present study in advance. The wall pressure profiles from the standard $k-\epsilon$ turbulent model and SST $k-\omega$ turbulent model are closer to the experimental data than those from other models. Referring to the past experimental and numerical researches [13], the standard $k-\epsilon$ turbulent model with enhanced wall function to treat the near-wall region was used in the present study. The diffusive fluxes were approximated using second-order central differences. The convergence criterion for momentum, k , ϵ , and energy equations is that maximum allowable residuals reach 10^{-4} for momentum, k , ϵ equation, and 10^{-6} for energy equation.

A FORTRAN program is coded to the infrared radiation characteristic analysis based on the Forward-Backward Ray Tracing Method (FBRTM). Ray-tracing is a statistical

method which traces rays of light from a source to a target, e.g., from the detector to an exhaust system, and then backtracks infrared radiation energy from target to source. The procedures of the program were referenced in the article [20]. In this paper, the infrared radiation of the inlet plane, internal surface, and plume of S-shaped nozzles is considered in the final signature analysis. For the external surface of nozzles shielded by the rear fuselage of aircraft, the external surface radiation is not represented and analyzed here.

A structural grid conducted by ICEM commercial software was used in all computational regions. A different grid density was treated in different regions. The inner flow in nozzles with complicated flow has finer grids than the flow far away from the core plume. A refined fine grid was used to deal with the wall boundary, shown in Figures 7(a) and 7(b). The minimum grid size is 0.05 mm, which is nearest the wall. Far away from the wall, the grid size increases with a ratio of 1.1. The wall neighboring-cell y^+ is confirmed

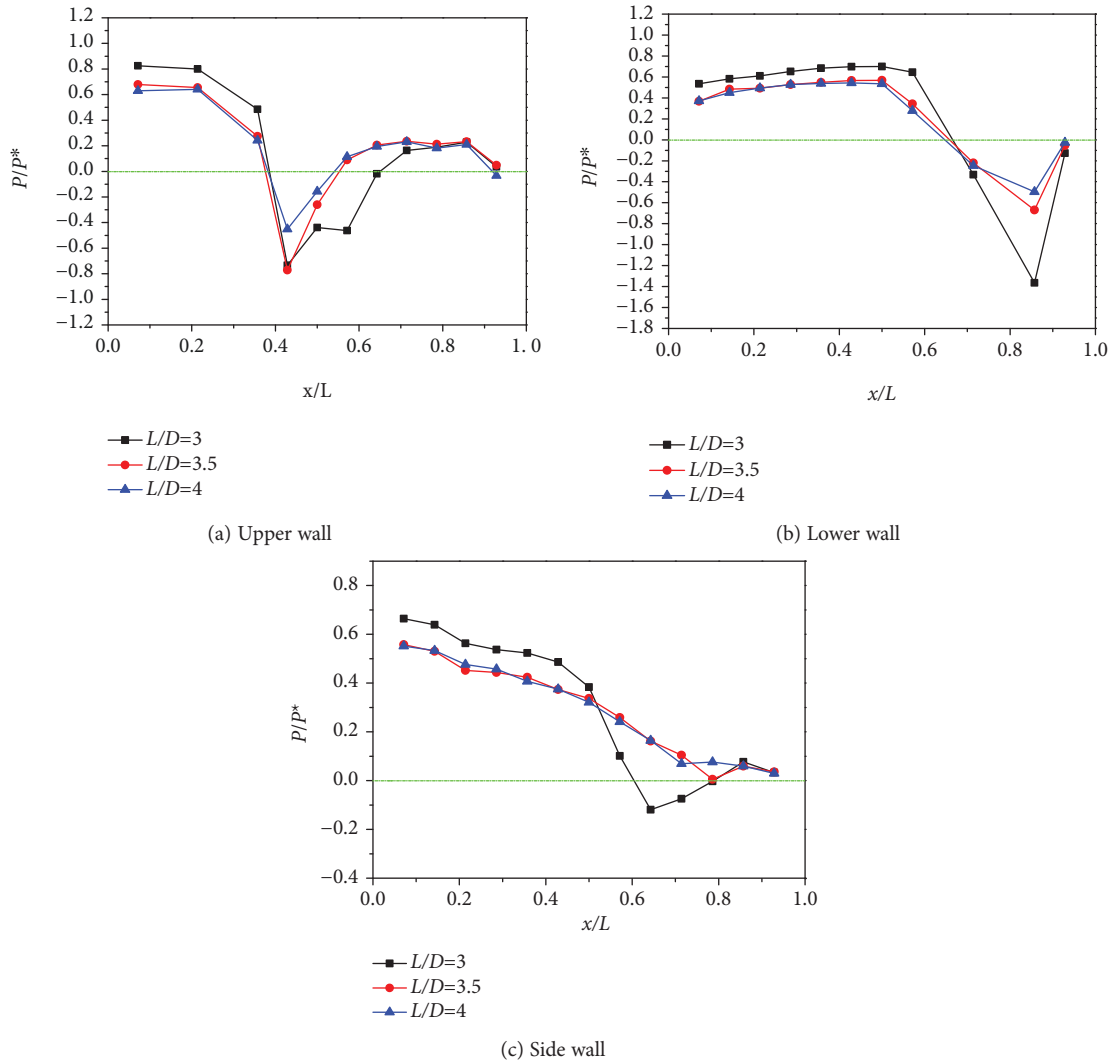


FIGURE 10: Effects of ratios of length to diameter on wall pressure.

under 5. In this computation, grid independency tests are per-conducted. As illustrated in Figures 7(c) and 7(d), when the grid number is beyond 3.5 million, the effect of the grid number on the area-weighted average pressure at the outlet of one S-shaped nozzle is very weak.

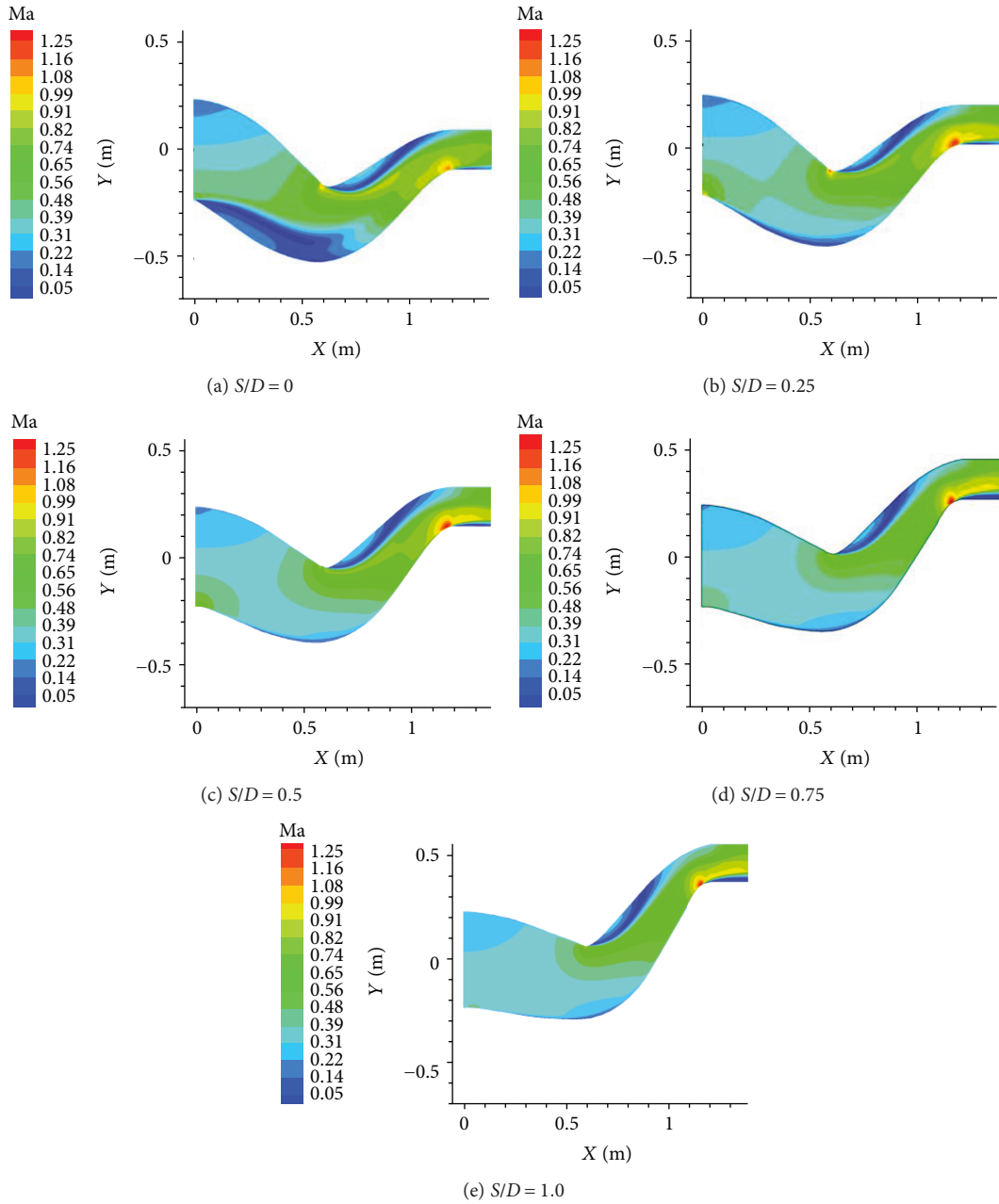
To describe and compare pressure distributions of various nozzles conveniently, the wall pressure was presented with nondimensional treatment based on inlet total pressure P^* . For nozzle of $S/D = 1$ and $L/D = 3.5$, the static pressures of the upper, lower, and side walls are compared in Figure 8. In general, the measured pressure agreed well with the numerical results in terms of both the trend and value. Thus, the aerodynamic numerical method is satisfied in accuracy.

5. Results and Discussions

5.1. Experimental Analysis. Figure 9 shows the effects of offset ratios on wall pressure at the equal inlet flow rate condition. There exists adverse pressure gradient which is supposed to

induce flow separation in nozzles. The first adverse pressure gradient arises from the first S turning of the upper wall. And the second pressure gradient appears on the second S turning of the lower wall. When the offset ratio increases from 0 to 0.5, the wall pressure does not seem to change obviously. For nozzle of $S/D = 1$, the whole wall pressure rise is remarkable because of the sharper turning of nozzles. This sharp turn of nozzles is supposed to gain more effectiveness to shield the line of sight, but it induces more loss of flow.

For the nozzle of $L/D = 3$, there are three positions where exist adverse pressure gradient that may induct flow separation and flow loss. The increase in the ratio of length to diameter L/D can obviously depress the adverse pressure gradient at the two S turning of the upper wall and lower wall for double S-shaped nozzles, which can be seen in Figure 10. However, the longer length of the nozzle means more space needed to house the nozzle and less effective load of the aircraft. The compromise should be taken between aerodynamic gain and weight issue.


 FIGURE 11: Ma number distributions on symmetric plane ($W/H = 3.3$, $L/D = 3$).

5.2. *Aerodynamic Performance Discussions.* To evaluate flow loss of double S-shaped nozzles quantitatively, the total pressure recovery coefficient is defined as follows,

$$\sigma = \frac{P_e^*}{P_{in}^*}. \quad (9)$$

Here, P_e^* and P_{in}^* are area-weighted average total pressure in outlet and inlet of nozzles.

Thrust coefficient C_f is another important performance character, which can be written as Equation (10). F_i is the

theoretical thrust of nozzles obtained from an isentropic expansion flow.

$$C_f = \frac{F}{F_i}, \quad (10)$$

The actual thrust produced by nozzles can be computed by Equation (11). Here, U and P_e are actual gas velocity and static pressure of nozzles at outlet. A_e is the area of the nozzle outlet.

$$F = \dot{m}U + (P_e - P_b)A_e. \quad (11)$$

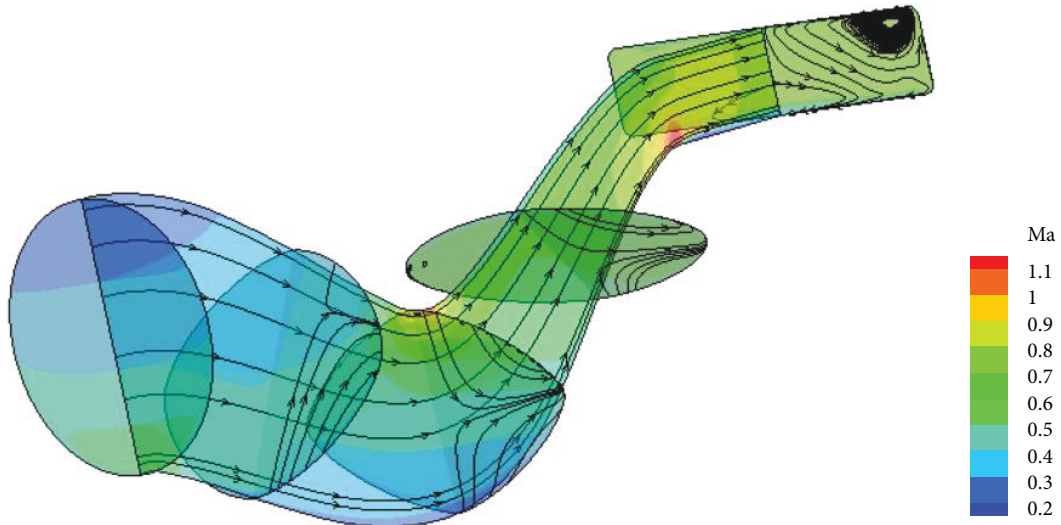
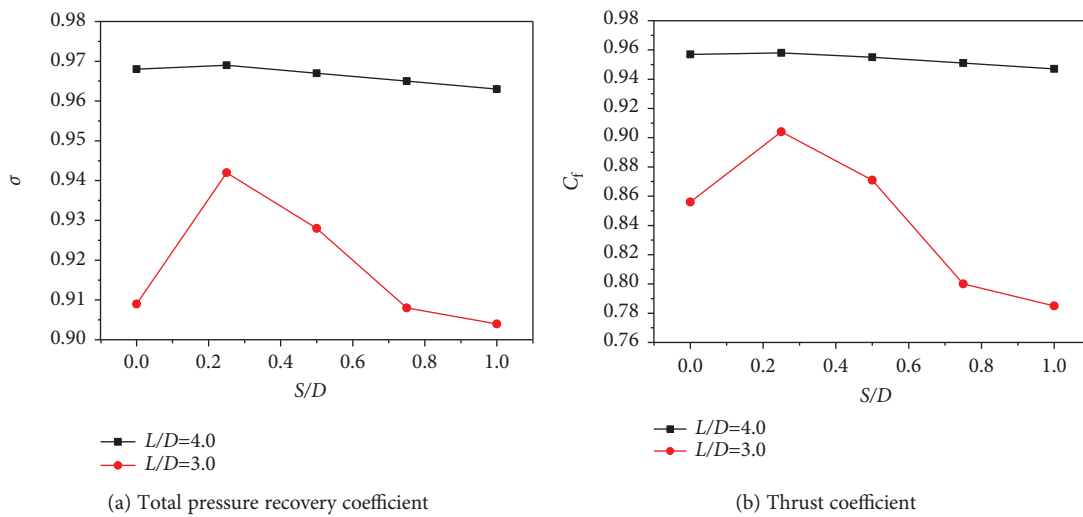
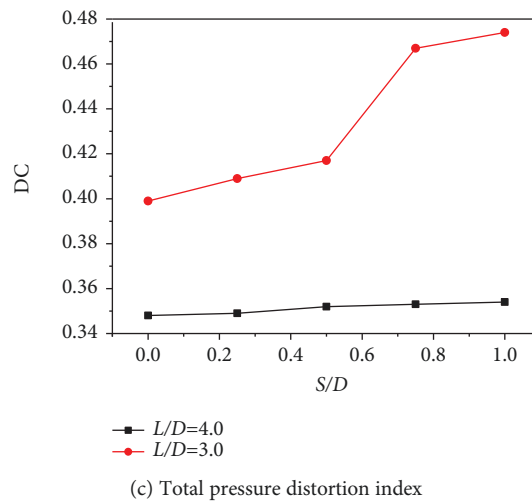


FIGURE 12: Streamlines of cross-sectional planes (colour denotes Mach number).



(a) Total pressure recovery coefficient

(b) Thrust coefficient



(c) Total pressure distortion index

FIGURE 13: Comparison of performances of nozzles with different S/D .

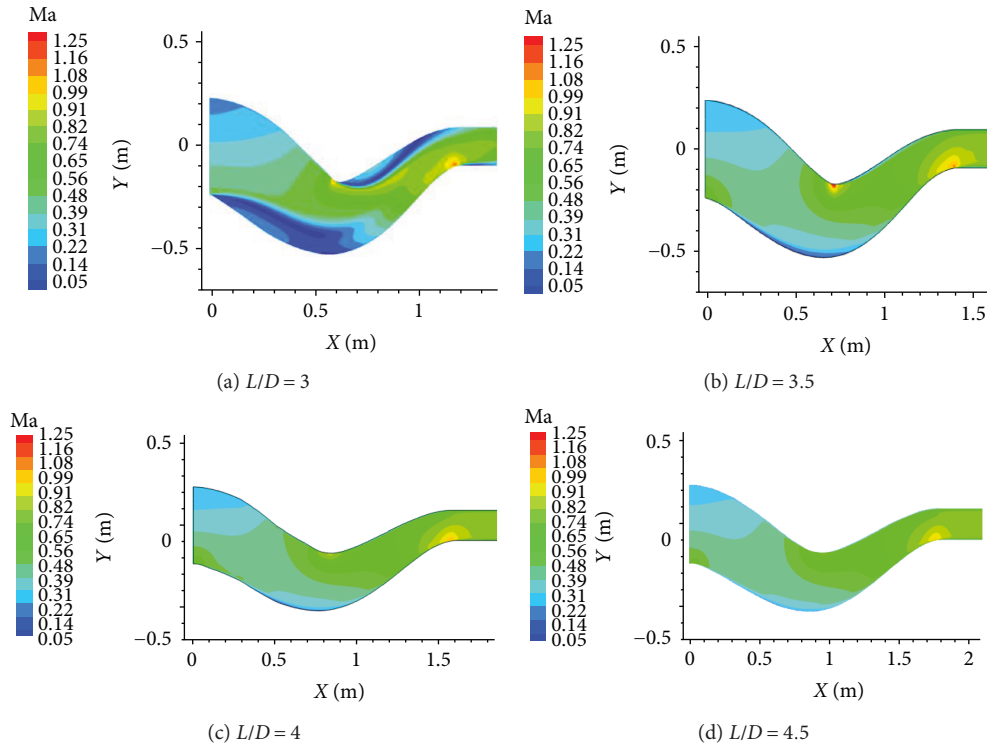


FIGURE 14: Mach number distributions on symmetric plane ($W/H = 3.3, S/D = 0$).

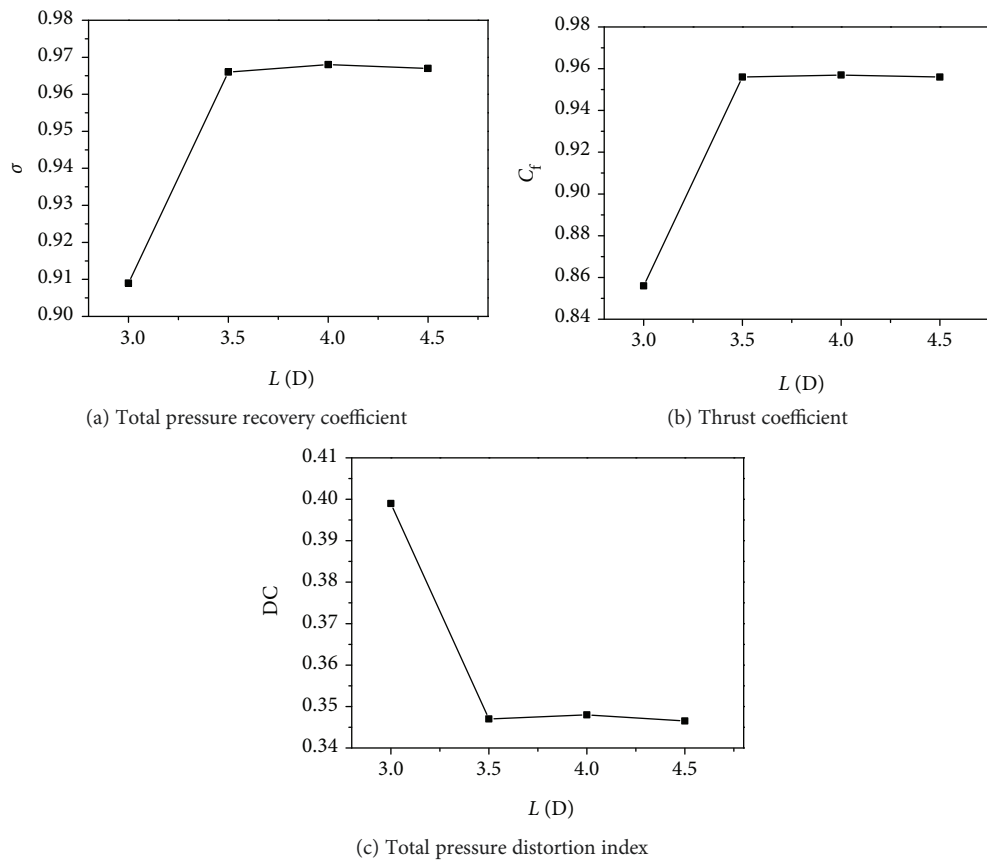


FIGURE 15: Comparison of performances of nozzles with different L/D ($W/H = 3.3, S/D = 0$).

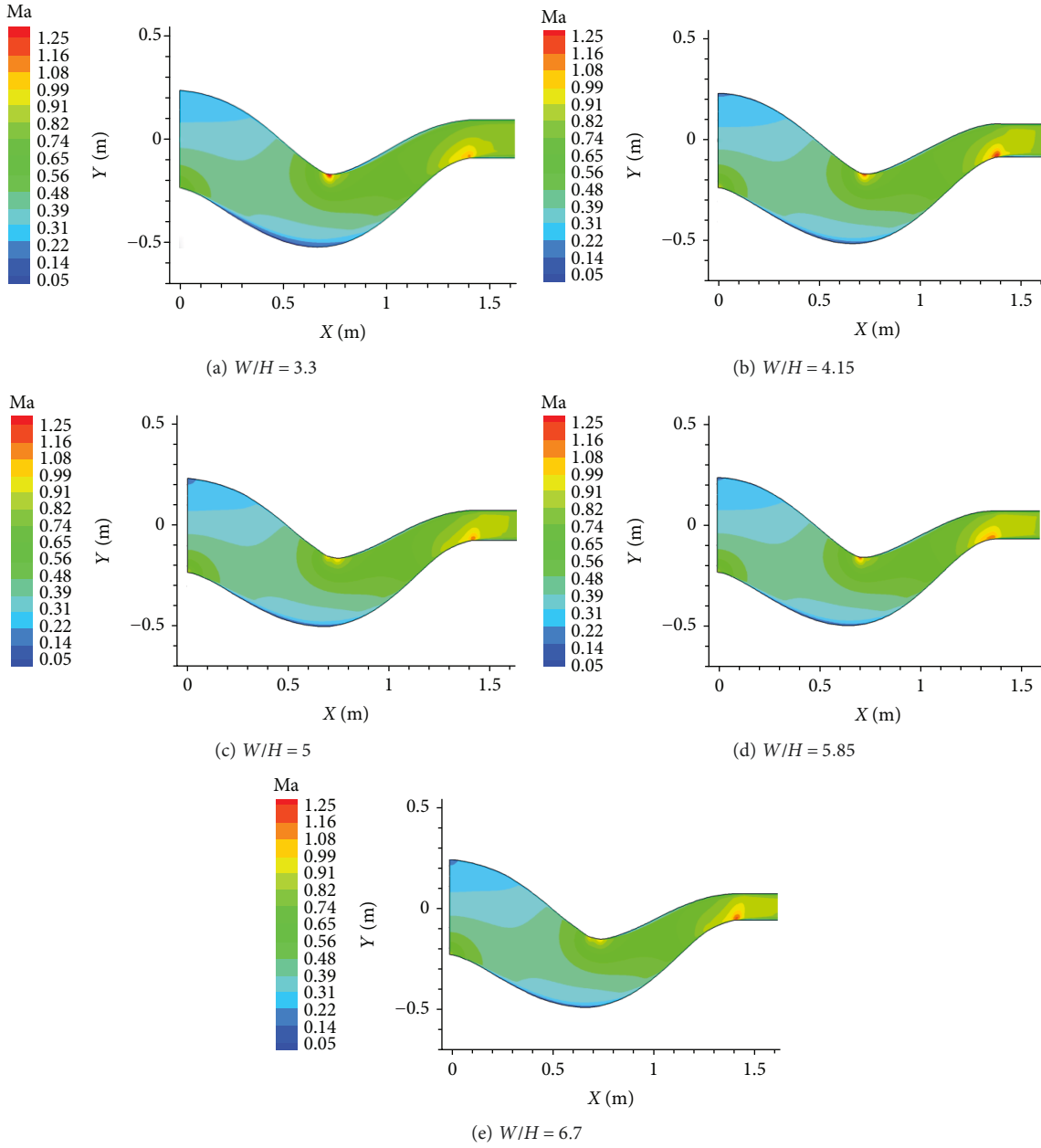


FIGURE 16: Mach number distributions on symmetric plane ($L/D = 3.5$, $S/D = 0$).

To estimate the pressure uniformity at the outlet of nozzles, total pressure distortion index DC is used and defined as

$$DC = \frac{P^*_{\max} - P^*_{\min}}{P^*_{\text{ave}}}, \quad (12)$$

where P^*_{\max} , P^*_{\min} , and P^*_{ave} are the maximum, minimum, and average total pressure at the outlet, respectively.

The flow accelerates from 0.35 Ma to 1.0 Ma through convergent double S-shaped nozzles, regardless of the offset ratios, which can be seen in Figure 11. For the baseline nozzle of $S/D = 0$, the nozzle turns down, and then turns up rapidly to satisfy the line-of-sight blockage

completely. This configuration induces the increase in nonuniformity of velocity at the inlet of nozzles. Downstream of the inlet, there is a low flow velocity zone adjacent to the downside wall. And the other low flow velocity zone exists after the first S-shaped turning close to the upper wall. After increasing the offset ΔY_2 of the second S-shaped turning, and decreasing the offset ΔY_1 of the first S-shaped turning, four other nozzles with increased offset ratio are formed to shrink the first low speed zone obviously. However, more space to settle down the nozzle is disadvantageous to integrate itself within the rear fuselage of aircraft.

To further understand the effect of twice turning of the inner flow, streamlines of cross-sectional planes are

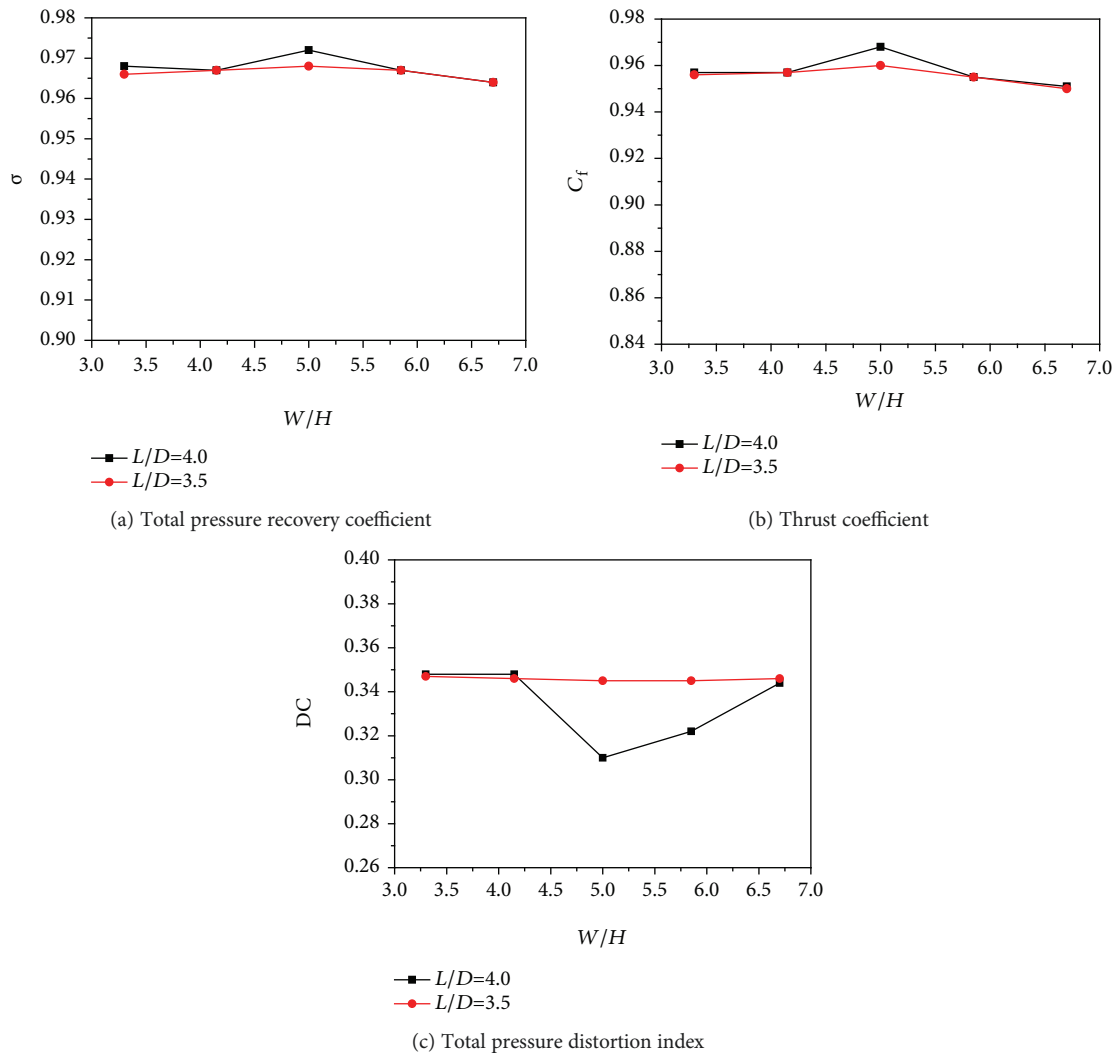


FIGURE 17: Comparison of performances of nozzles with different W/H ($S/D = 0$).

demonstrated in Figure 12. Except for the accelerating phenomenon along the nozzle passage, secondary flows are induced in the nozzle, which is one of the main causes of flow loss. At the first S turning, the upper wall provides centrifugal force to cause a downward movement. At the second S turning, the lower wall provides centrifugal force to cause an upward movement.

Figure 13 shows the aerodynamic performances in the function of offset ratio S/D . For nozzles of $L/D = 3$, with the increase in offset ratio, the total pressure recovery coefficient and thrust coefficient are improved initially, but then drop rapidly. The total pressure distortion index always increases. Overall, the nozzle with an offset ratio $S/D = 0.25$ has better performances. For nozzles of $L/D = 4$, the offset ratio seldomly has any effects on aerodynamic performances compared to nozzles of $L/D = 3$. At the same offset ratio S/D , the increase in nozzle length means the turning of flow is more modest. Thus, the aerodynamic performance of nozzles is supposed to be improved.

The Mach number distribution on the symmetric plane of four nozzles with different ratios of length to diameter is

compared in Figure 14. Due to the increase in nozzle length, it is taken for granted that the aerodynamic loss is reduced for the modest turning flow. For the nozzle of $L/D = 4.5$, the recirculation zone cannot be recognized clearly in Figure 14(d), and flow velocity tends to be uniform on the transverse section. As shown in Figure 15 of performances, after the L/D increases from 3.0 to 3.5, the total pressure recovery coefficient and the thrust coefficient rise as much as 6.3% and 11.7%, respectively. And the total pressure distortion index drops by 15%. It is interesting that the three factors would hardly change once the L/D exceeds 3.5. The increase in nozzle length induces weight penalty, but is not helpful for the enhancement of aerodynamic performances.

As shown in Figure 16, the change in the aspect ratio has trivial effects on the inner flow structure and Mach number distributions. As a result, the aspect ratio has no significant effects on aerodynamic performances for S-shaped nozzles in the parameter range of this study, which can be proven by Figure 17. The nozzle of $W/H = 5$ has relatively higher performances which can be observed from streamlines and total pressure distributions on the outlet shown in

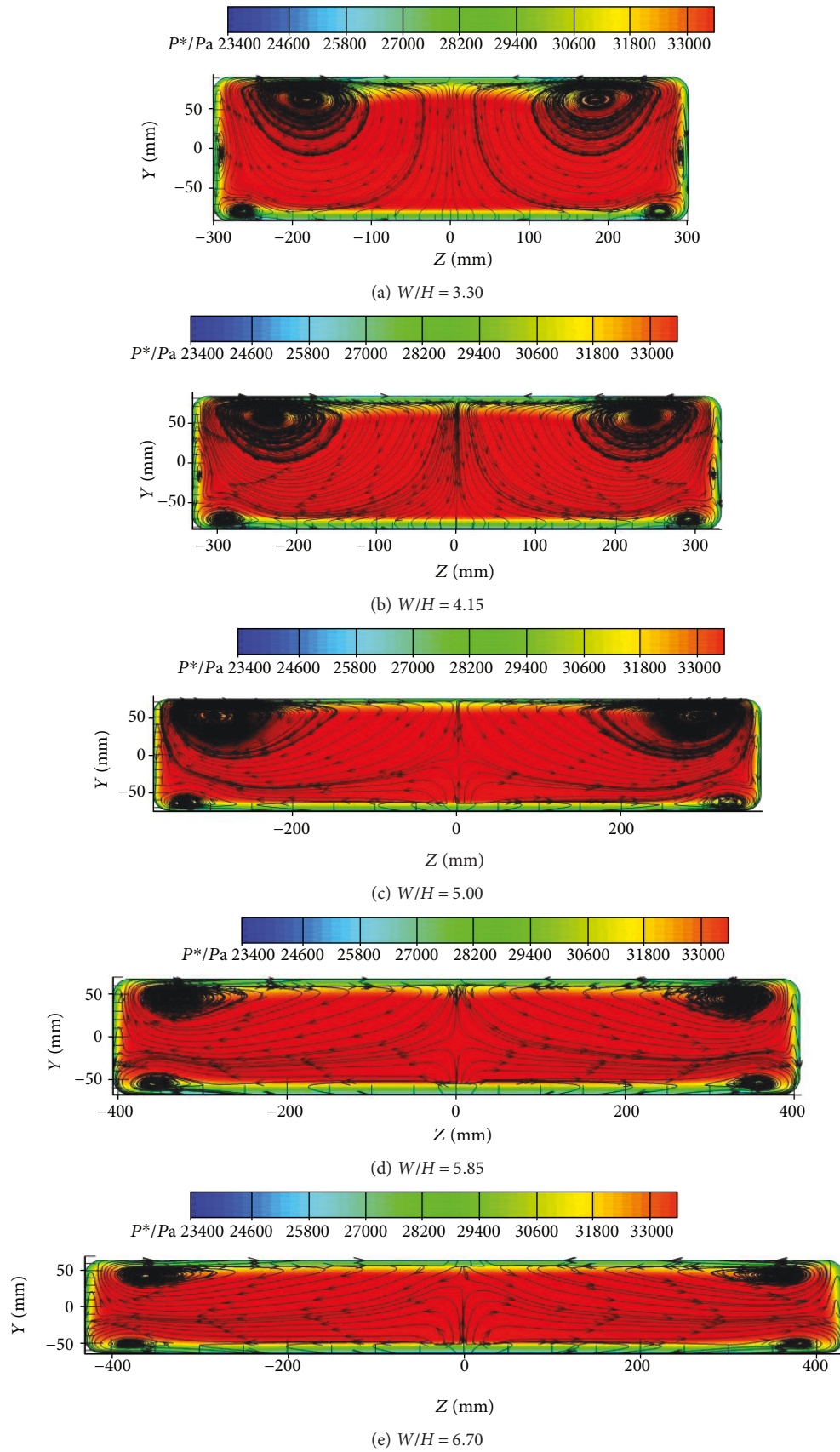


FIGURE 18: Streamlines and total pressure distributions at outlets ($L/D = 4.0, S/D = 0$).

Figure 18. Except for the friction loss, vortice pairs present at the nozzle outlet are an important factor to cause flow loss. For the nozzle of $W/H = 3.3$, three vortice pairs appear on the side, upper, and lower walls. With the increase in the aspect ratio, flow is restricted by the upper and lower walls. Two vortex pairs are squeezed to deform, and their sizes are reduced. Simultaneously, one pair of vortices near the side wall diminishes due to the lack of space to form. Thus, the loss induced by vortices is reduced. The increase in the aspect ratio enlarges the perimeter of the rectangular outlet, which induces the enhancement of friction and free shear. So, the flow loss will be augmented due to the further enlargement of W/H .

5.3. Infrared Radiation Characteristics. Due to the 2D geometric characteristics, two planes were used to discuss the $3\ \mu\text{m} - 5\ \mu\text{m}$ infrared radiation distribution for nozzles. The horizontal plane (xoz plane) and vertical plane (xoy plane) have orthogonality with the detecting points located on the perimeter of the circle in Figure 19.

To evaluate the infrared radiation of the nozzle, the inlet plane and internal surface of double S-shaped nozzles are treated as a gray body with emissivity of 0.8. Infrared radiation of the inlet plane, internal surface, and plume of nozzles can be calculated separately by the program used in this study. In this paper, overall radiation includes the inlet plane, internal surface, and plume radiation. At any detecting points, a maximum value is chosen to nondimensionalize radiation intensity I_r . An axis-symmetric nozzle which has the same inlet and outlet area as double S-shaped nozzles is used as the baseline.

On the horizontal plane, 0 degree denotes the rear direction horizontally. And ± 90 degree denotes both side direction of nozzles. It can be shown in Figure 20 that distributions of both overall radiation and plume are symmetric on the horizontal plane because of the geometric symmetry. In contrast to the axis-symmetric nozzle, the overall radiation of double S-shaped nozzles has excellent infrared suppression ability by about 50% decline at the 0 degree perspective, which can be observed in Figure 20(a). The radiation of various parts of nozzles is also obtained separately. The radiation of the inlet of the axis-symmetric nozzle is about 40% of the overall radiation. The radiation of the inlet of double S-shaped nozzles is 0% of the overall radiation. Compared with double S-shaped nozzles, if the inlet plane radiation of the axis-symmetric nozzle was separated from its overall radiation, the rest part of the axis-symmetric nozzle is equivalent to the overall radiation of double S-shaped nozzles. Figure 21 shows the inlet and wall temperature of various nozzles. Obviously, the inlet of double S-shaped nozzles cannot be seen directly at rear view. In fact, it cannot be observed at any view because of the perfect shield. At the two inflection points of double S-shaped nozzles, accelerating flow causes the wall temperature to decrease slightly, which can be also observed in Figure 21.

Compared to the axis-symmetric nozzle, double S-shaped nozzles with a rectangular outlet present the good ability of plume radiation decline by 60%-70% (shown in Figure 20(b)). The increase in aspect ratios leads to the

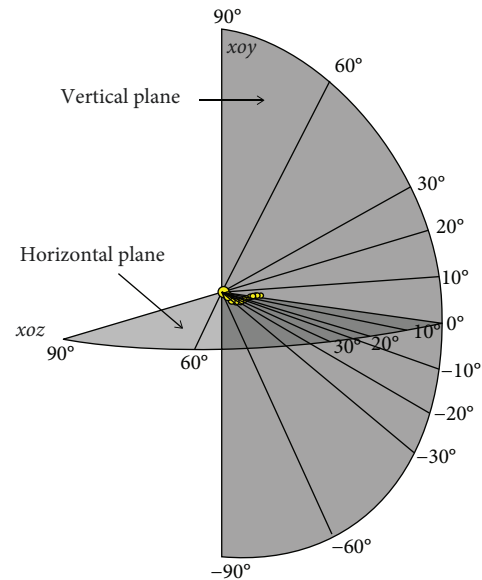


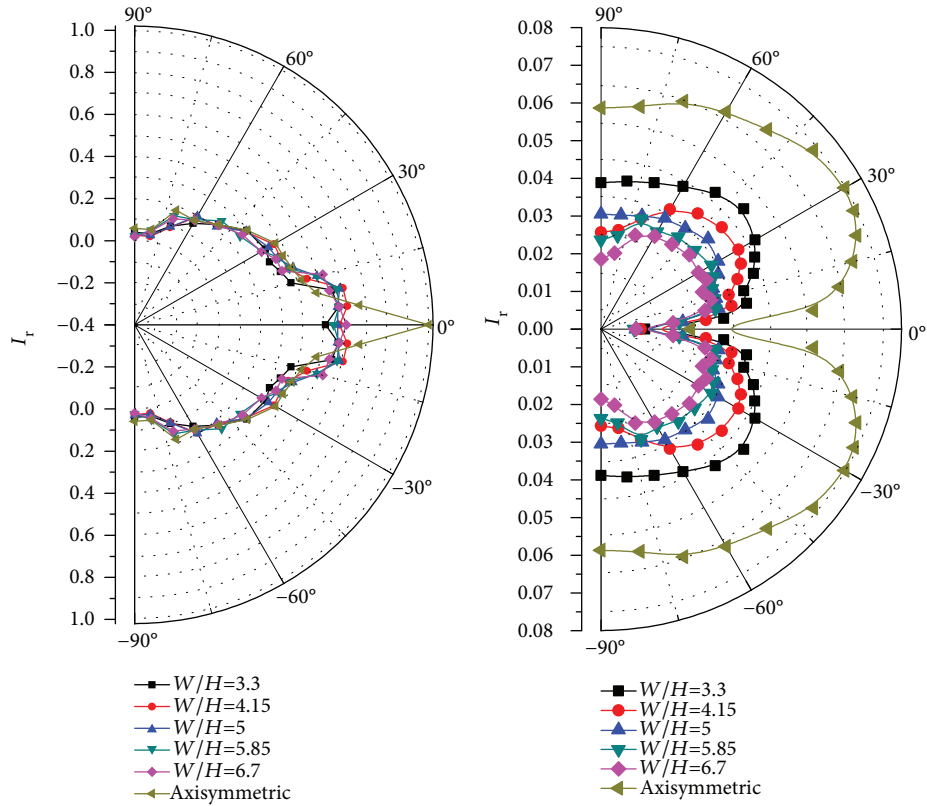
FIGURE 19: The detecting point located on the horizontal and vertical planes.

decrease in plume infrared radiation due to better mixing between plume and atmosphere. It can be demonstrated by plume temperature and the length of core flow shown in Figure 22.

The contribution of plume radiation in the total IR signature can be analyzed by comparing Figures 20(a) and 20(b). At the rear aspect (0°), plume radiation is about 2%-3% of the overall radiation for the axis-symmetric nozzle. At the side aspect ($\pm 90^\circ$), the internal surface of nozzles cannot be seen; thus, plume radiation is 100% of the overall radiation. At other angles, plume radiation is about 10%-20% of the overall radiation. It concludes that double S-shaped nozzles have a high infrared suppression performance because of the radiation shield from the nozzle inlet and its upstream components. The aspect ratio seems to have only slight effects on the overall radiation level and its distribution at most detecting perspectives because of the low contribution of plume radiation.

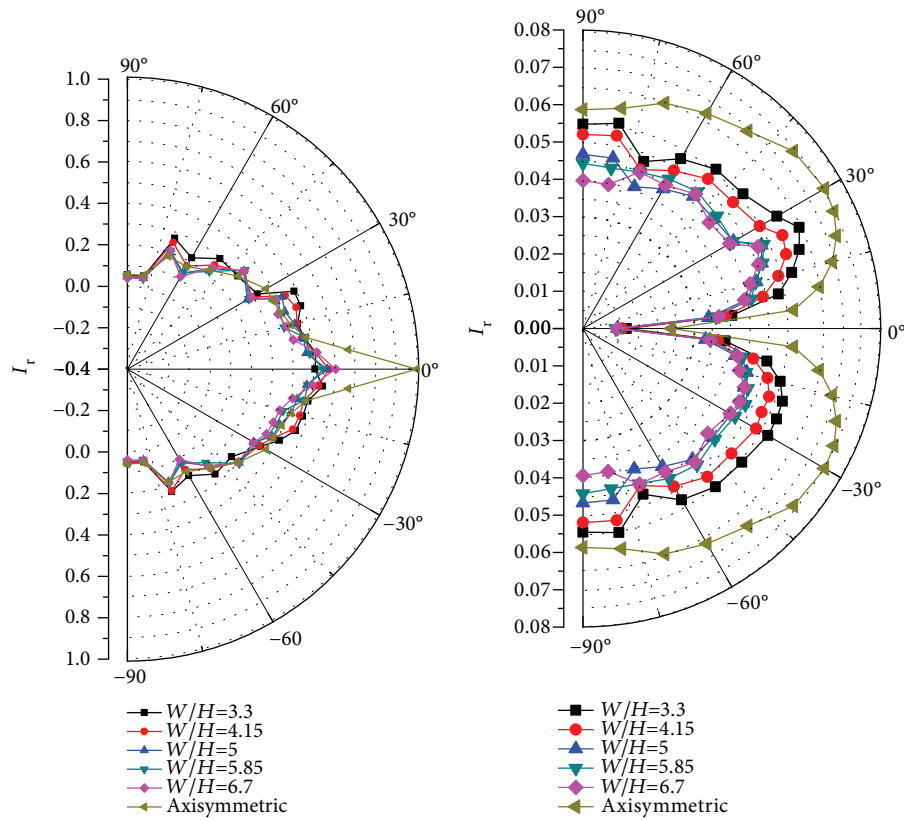
The infrared radiation on the vertical plane exhibits the same characteristics as that on the horizontal plane.

Figure 23 shows the infrared radiation distribution of exhaust nozzles in the band of $3-5\ \mu\text{m}$ with varying offset ratios of S/D . Compared to the axis-symmetric nozzle, the double S-shaped nozzle of $S/D = 1$ has the maximum suppression of plume radiation by 50% and 40% on the horizontal and vertical planes, respectively. With the increase in offset ratio, the plume radiation initially increases, but then declines. It can be explained by the length of core flow shown in Figure 24. For the nozzle of $S/D = 0.25$, the length of core flow reaches the maximum. The offset ratio is hardly effective on the overall radiation. The increase in offset ratio causes the angle to increase corresponding to the overall radiation peak. Compared to the axis-symmetric nozzle, the overall radiation of S-shaped nozzles is suppressed by above 50% at 0 degree view on any detecting plane.



(a) Overall radiation on the horizontal plane

(b) Plume radiation on the horizontal plane



(c) Overall radiation on the vertical plane

(d) Plume radiation on the vertical plane

FIGURE 20: Infrared radiation of exhaust systems in the band of 3-5 μm varying W/H .

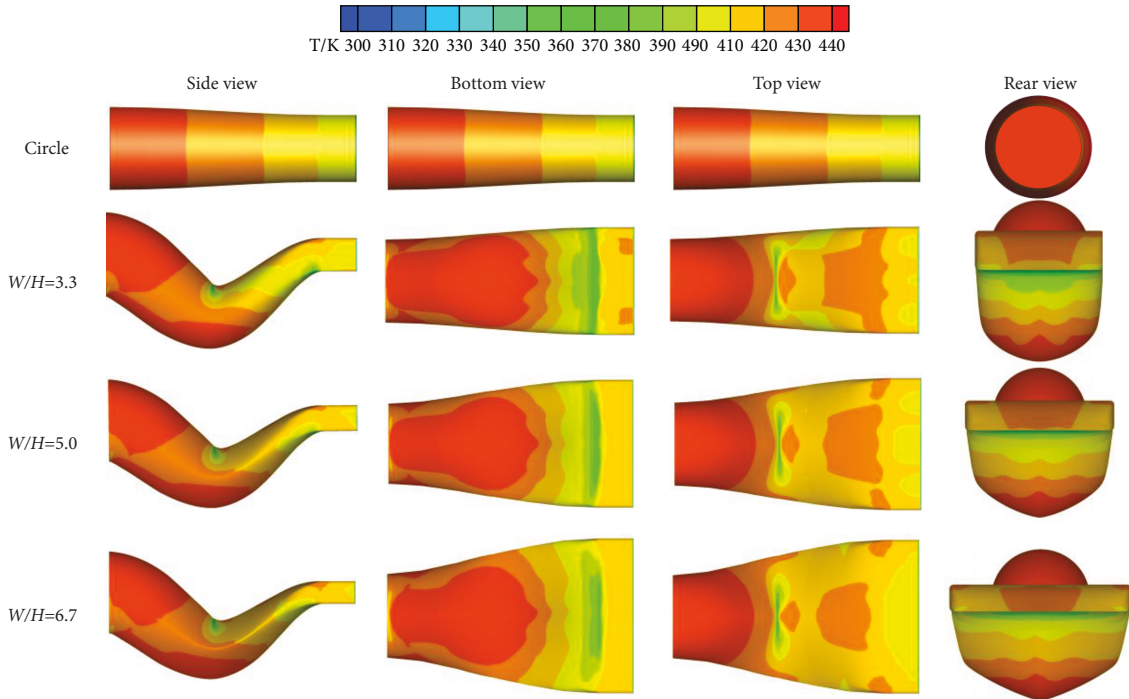


FIGURE 21: Wall temperature varying W/H .

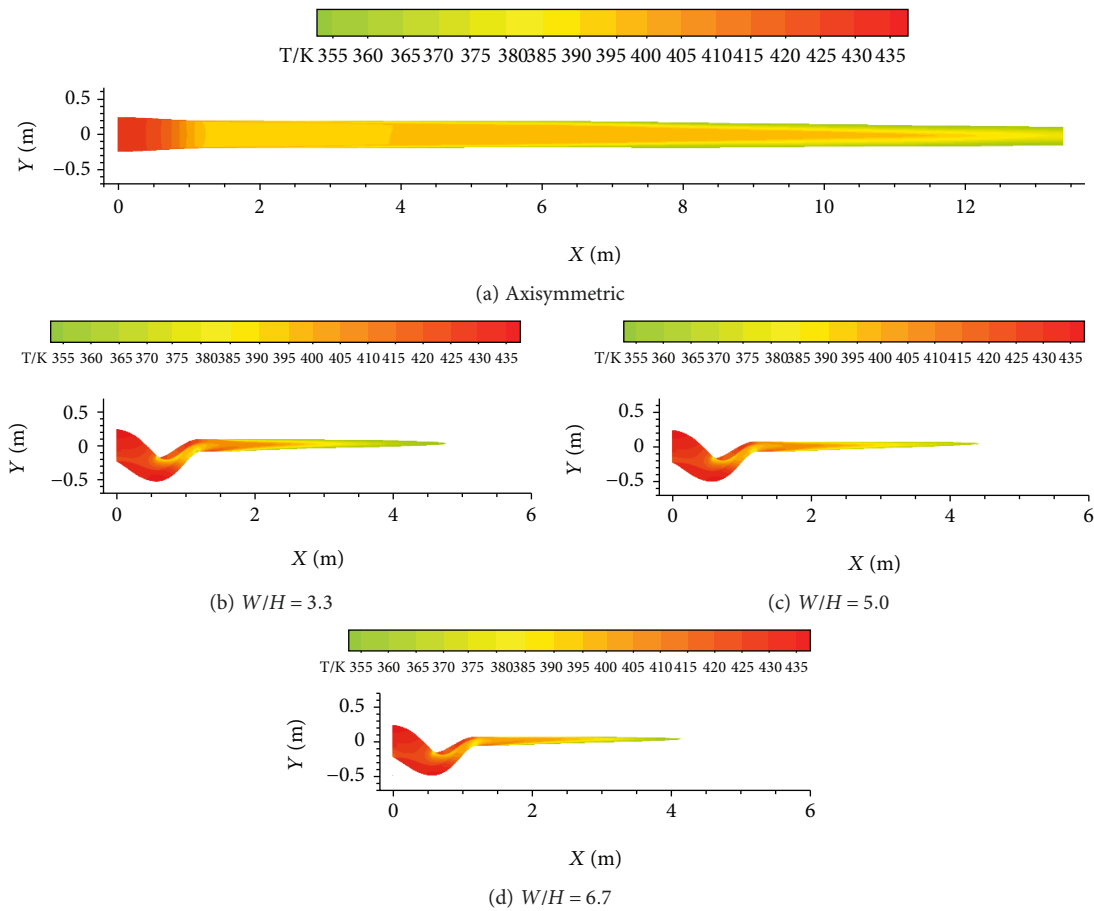
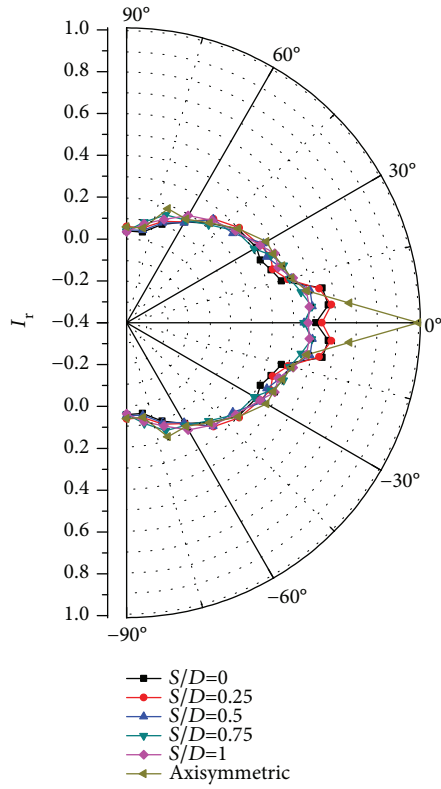
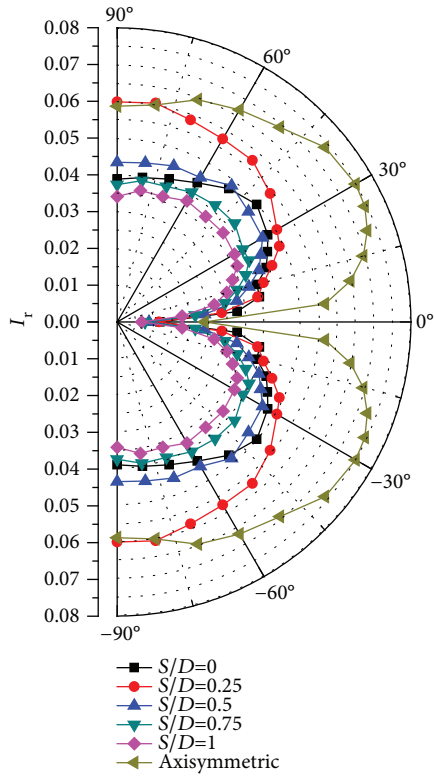


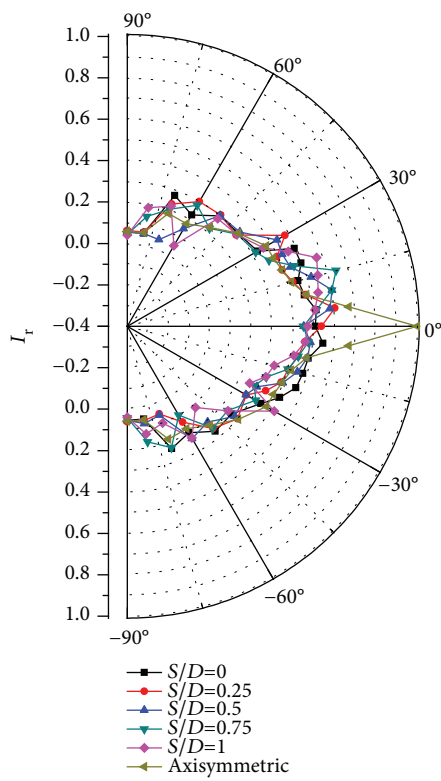
FIGURE 22: Static temperature on the symmetrical section varying W/H .



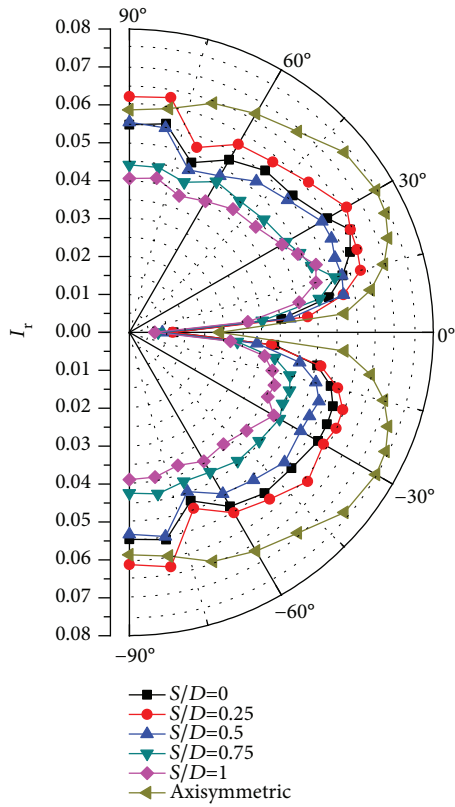
(a) Overall radiation on the horizontal plane



(b) Plume radiation on the horizontal plane



(c) Overall radiation on the vertical plane



(d) Plume radiation on vertical plane

FIGURE 23: Infrared radiation of exhaust systems in band of 3-5 μm varying S/D .

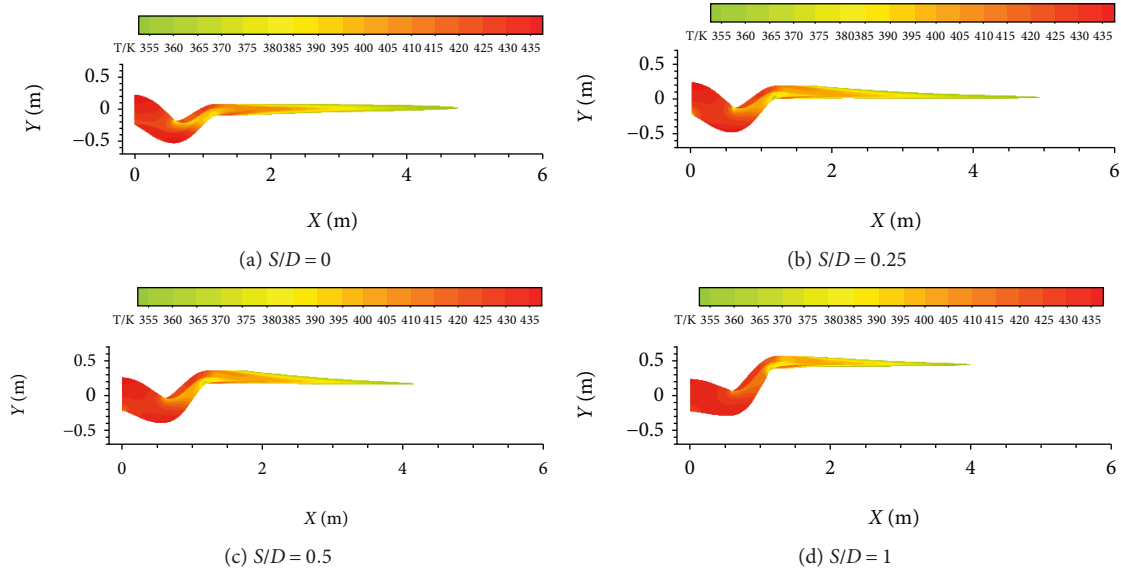


FIGURE 24: Static temperature on the symmetrical section above 350 K varying S/D .

In addition, the ratio of length to diameter has no obvious effects on radiation of S-shaped nozzles, which can be seen in Figure 25. Even if the ratio of length to diameter changes a lot, the projected area of internal surface of double S-shaped nozzles could not be changed at any angle of observation.

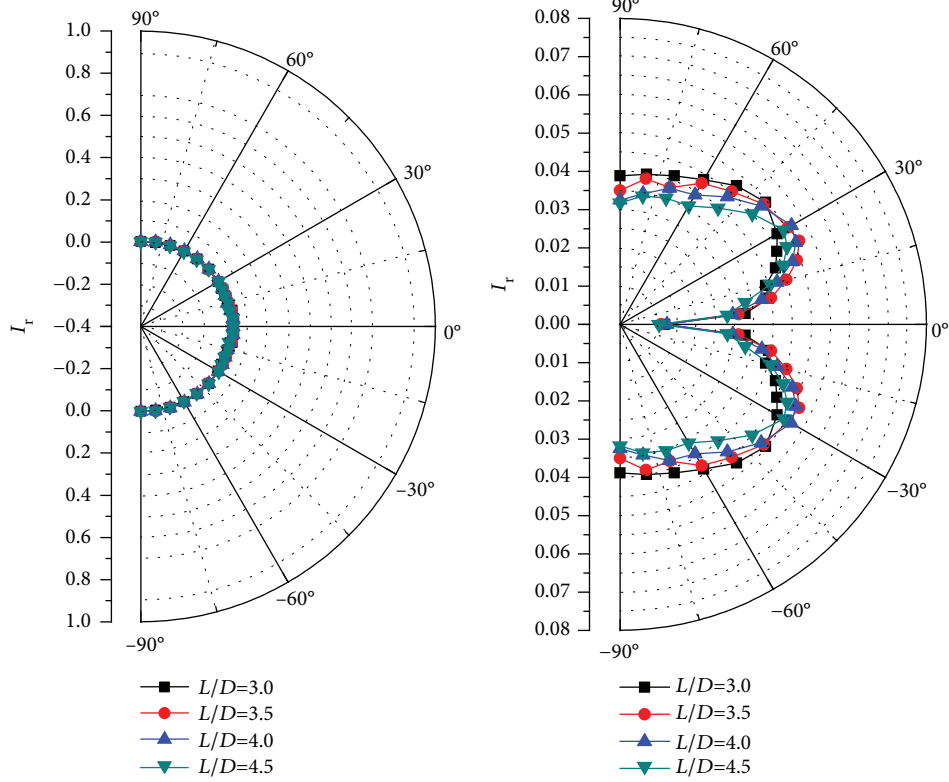
6. Conclusions

This study demonstrates integrated procedures to form a double S-shaped nozzle based on the complete line-of-sight shielding principle. Using this method, a series of nozzles were designed to facilitate aerodynamic experiments and numerical simulations. Some rules and findings were concluded as the following.

- (1) By the method introduced in this paper, the geometric shape of double S-shaped nozzles with a super-elliptical transverse section can be easily established with the input of inlet and outlet parameters of nozzles. This solution is highly efficient and adaptive in modeling complex geometric configurations
- (2) In the range of geometric parameters investigated in this paper, the total pressure recovery coefficient and thrust coefficient increase initially, but then drop rapidly with the increase in offset ratios. The total pressure distortion index is gradually increased. Compared to the nozzle of $S/D=0$ and $S/D=1$, the nozzle of $S/D=0.25$ has a better thrust coefficient by 5.6% and 15.2% increase, respectively. That is to say, for different nozzles, there exists an optimal offset ratio to achieve the best aerodynamic performances
- (3) In the passage of nozzles, a reverse flow zone on the turning point caused by adverse pressure gradient is

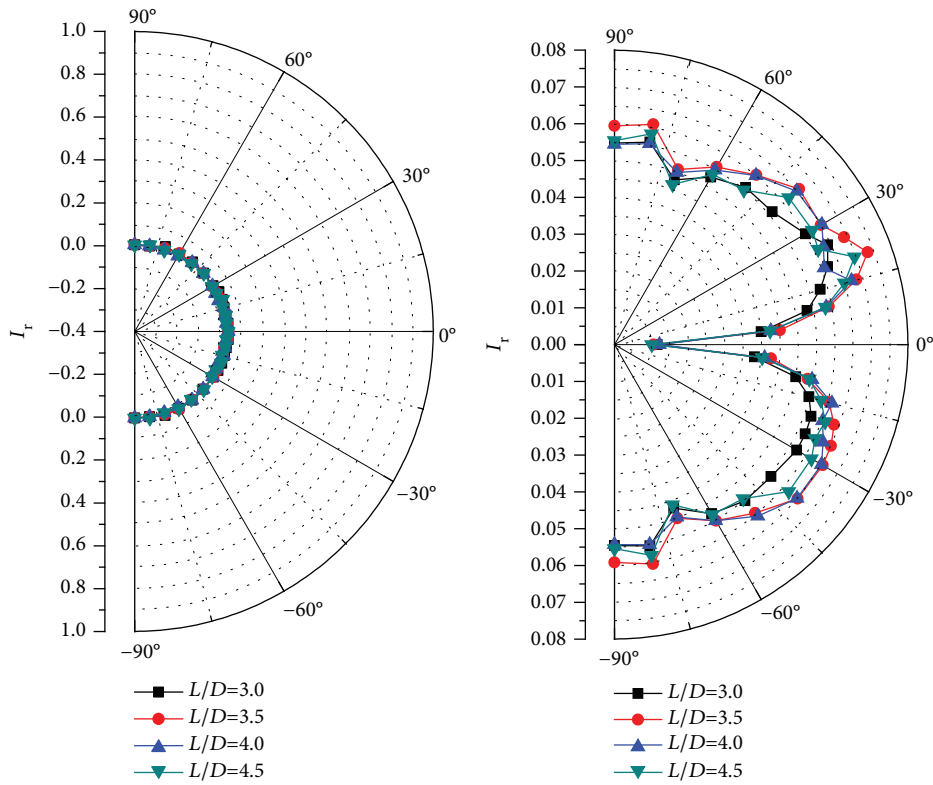
a significant factor to increase aerodynamic loss. For the short length nozzle of $L/D=3$, the nonuniform inlet velocity profile and recirculation are obviously seen. After increasing L/D from 3 to 3.5, the total pressure recovery coefficient and thrust coefficient are enhanced by 6.3% and 11.7%, respectively. However, the aerodynamic performances cannot be improved with further increase of L/D

- (4) For the nozzle with minor aspect ratio, there appear three vortex pairs on the side, upper, and lower walls of the rectangle outlet. Viscous loss caused by large dimensional streamwise vortices dominates the overall loss of nozzles. For the nozzle with a major aspect ratio, two vortex pairs located near the upper and lower walls are squeezed to deform and their sizes are reduced. Simultaneously, one pair of vortices near the side wall diminishes due to the lack of space. Thus, the loss induced by vortices is reduced. The increase in aspect ratio further increases the perimeter of the rectangular outlet, which induces the enhancement of friction and free shear. So, the flow loss will be augmented due to the further enlargement of W/H
- (5) The increases in aspect ratios and offset ratios are effective to suppress plume radiation, but they have fewer effects on overall radiation. No matter what the parameters of double S-shaped nozzles are changed to, the nozzles have significant stealth ability. Compared to circular nozzles, the double S-shaped nozzles reduced infrared radiation by over 50%
- (6) In summary, a balance between aerodynamic performances and infrared radiation suppression can be reached for double S-shaped nozzles



(a) Overall radiation on the horizontal plane

(b) Plume radiation on the horizontal plane



(c) Overall radiation on the vertical plane

(d) Plume radiation on the vertical plane

FIGURE 25: Infrared radiation of exhaust systems in the band of 3-5 μm varying L/D .

Nomenclature

L :	Length (m)
p :	Static pressure (Pa)
P^* :	Total pressure (Pa)
A :	Area (m^2)
AR :	Aspect ratio
ϵ :	Turbulent dissipation rate (m^2/s^3)
k :	Turbulent kinetic energy (m^2/s^2)
R :	Radius (m)
NPR :	Pressure ratio of nozzle
a :	Long axis of super ellipse (m)
b :	Short axis of super ellipse (m)
ΔY :	Offset of nozzle (m)
σ :	Total pressure recovery coefficient
C_f :	Thrust coefficient
F :	Thrust (N)
m :	Mass flow rate (kg/s)
DC :	Total pressure distortion index
I :	Radiation intensity (W/Sr)
T :	Temperature (K)
S :	Offset ratio of nozzle
n :	Exponent of super ellipse
Ma :	Mach number.

Subscripts

e :	Exit of nozzle/equivalent
in :	Inlet of nozzle
b :	Atmosphere
λ :	Wavelength (μm)
1:	The first S-shaped segment
2:	The second S-shaped segment
3:	The straight segment
i :	Theoretical
max :	Maximum
min :	Minimum
ave :	Average
r :	Relative.

Data Availability

The data used to support the findings of this study are included within the article.

Conflicts of Interest

The authors declare that they have no conflicts of interest.

Acknowledgments

The authors gratefully acknowledge the financial support for this project from the National Natural Science Foundation of China (No. U1508212).

References

- [1] R. E. Ball, *The Fundamentals of Aircraft Combat Survivability Analysis and Design*, AIAA Education Series, AIAA, Reston, VA, USA, 2nd edition, 2003.
- [2] D. Howe, "Introduction to the basic technology of stealth aircraft: part 1—basic considerations and aircraft self-emitted signals (passive considerations)," *Journal of Engineering for Gas Turbines and Power*, vol. 113, no. 1, pp. 75–79, 1991.
- [3] G. A. Rao and S. P. Mahulikar, "Integrated review of stealth technology and its role in airpower," *The Aeronautical Journal*, vol. 106, no. 1066, pp. 629–641, 2002.
- [4] J. R. Carlson and K. S. Abdol-Hamid, "Prediction of internal performance for two-dimensional convergent-divergent nozzles," in *27th Joint Propulsion Conference, Joint Propulsion Conferences*, pp. 91–2369, Sacramento, CA, USA, June 1991.
- [5] F. J. Capone and K. A. Deere, "Transonic investigation of two-dimensional nozzles designed for supersonic cruise aircraft," in *37th Joint Propulsion Conference and Exhibit*, Salt Lake City, UT, USA, July 2001.
- [6] M. C. Gridley and S. H. Walker, "Inlet and nozzle technology for 21st century fighter aircraft," in *ASME 1996 International Gas Turbine and Aeroengine Congress and Exhibition*, p. 8, Birmingham, UK, June 1996.
- [7] C. H. An, D. W. Kang, S. T. Baek, R. S. Myong, W. C. Kim, and S. M. Choi, "Analysis of plume infrared signatures of S-shaped nozzle configurations of aerial vehicle," *Journal of Aircraft*, vol. 53, no. 6, pp. 1768–1778, 2016.
- [8] P. Rajkumar, T. Chandra Sekar, A. Kushari, B. Mody, and B. Uthup, "Flow characterization for a shallow single serpentine nozzle with aft deck," *Journal of Propulsion and Power*, vol. 33, no. 5, pp. 1130–1139, 2017.
- [9] L. Du, Y. Liu, and T. Li, "Numerical predictions of scarfing on performance of S-shaped nozzle with asymmetric lobe," *Journal of Propulsion and Power*, vol. 31, no. 2, pp. 604–618, 2015.
- [10] X. Gao, Q. Z. Yang, H. Zhou, and J. N. He, "Numerical simulation on the infrared radiation characteristics of S-shaped nozzles," *Applied Mechanics and Materials*, vol. 482, pp. 282–286, 2013.
- [11] C. C. Liu, H. H. Ji, N. Li, and L. Z. Lin, "Numerical simulation on infrared radiant characteristics of 2D S-nozzles," *Journal of Engineering Thermophysics*, vol. 31, no. 9, pp. 1567–1570, 2010.
- [12] C. C. Liu, H. H. Ji, W. Huang, and F. F. Yang, "Numerical simulation on infrared radiation characteristics of serpentine 2-D nozzle," *Journal of Aerospace Power*, vol. 28, no. 7, pp. 1482–1488, 2013.
- [13] X. L. Sun, Z. X. Wang, L. Zhou, J. W. Shi, and Z. W. Liu, "Experimental and computational investigation of double serpentine nozzle," *Proceedings of the Institution of Mechanical Engineers, Part G: Journal of Aerospace Engineering*, vol. 229, no. 11, pp. 2035–2050, 2015.
- [14] X. L. Sun, Z. X. Wang, L. Zhou, Z. W. Liu, and J. W. Shi, "Influences of design parameters on a double serpentine convergent nozzle," *Journal of Engineering for Gas Turbines and Power*, vol. 138, no. 7, pp. 072301–072301-16, 2016.
- [15] W. Cheng, Z. Wang, L. Zhou, X. Sun, and J. Shi, "Influences of shield ratio on the infrared signature of serpentine nozzle," *Aerospace Science and Technology*, vol. 71, pp. 299–311, 2017.
- [16] M. Johansson, "Propulsion integration in an UAV," in *24th AIAA Applied Aerodynamics Conference, Fluid Dynamics and Co-located Conferences*, San Francisco, CA, USA, June 2006.
- [17] W. Collie, R. Burgun, S. Heinzen et al., "Advanced propulsion system design and integration for a turbojet powered

unmanned aerial vehicle,” in *41st Aerospace Sciences Meeting and Exhibit*, Reno, Nevada, January 2013.

- [18] S. C. Darrell, “Effect of geometry on exit temperature from serpentine exhaust nozzles,” in *53rd AIAA Aerospace Sciences Meeting*, Kissimmee, FL, USA, January 2015.
- [19] C. C. Lee, S. Louis, and C. Boedicker, “Subsonic diffuser design and performance for advanced fighter Aircraft,” in *Aircraft Design Systems and Operations Meeting*, pp. 85–3037, Colorado Springs, CO, USA, October 1985.
- [20] Y. Shan and J. Z. Zhang, “Numerical investigation of flow mixture enhancement and infrared radiation shield by lobed forced mixer,” *Applied Thermal Engineering*, vol. 29, no. 17-18, pp. 3687–3695, 2009.



Hindawi

Submit your manuscripts at
www.hindawi.com

